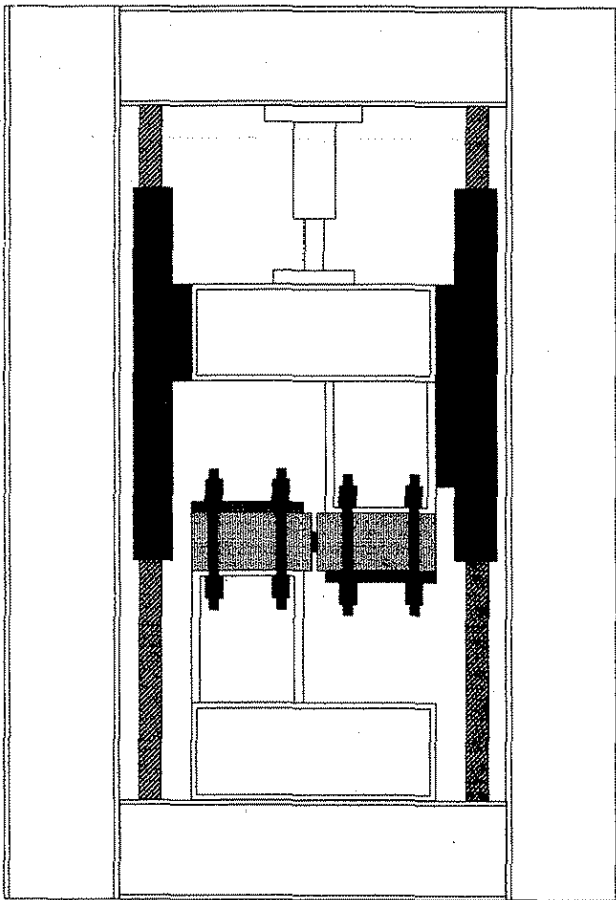Max L. Porter   Eric A. Lorenz   Kasi P. Viswanath
Bruce A. Barnes   Michael D. Albertson

Thermoset Composite Concrete Reinforcement

May 1992

Part 1   final

report

Engineering Research Institute
Iowa State University

Disclaimer

The contents of this report do not represent a warranty of the products used on behalf of the State of Iowa, Iowa State University, Iowa Department of Transportation, Highway Research Board, or the authors. The opinions, findings, and conclusions expressed in this publication are those of the author and not necessarily those of the Highway Division of the Iowa Department of Transportation. Engineering data, design, details, with recognized professional principals and practices are for general information only. The data, designs, and suggested conclusions should not be used without first securing competent advice with respect to the suitability for any given application. The responsibility for the use of information in this report remains with the user. This report is for information purposes and is made available with the understanding that it will not be cited without the permission of the authors.

Preface

The final report submitted to the Iowa Department of Transportation will be broken in two parts (Part 1 and Part 2). The final report will fulfill all requirements of the Scope and Objective given in the research proposal [1]. Part 1 of this report covers the comparison of unaged fibercomposite and steel dowels and derivation of the appropriate theoretical model for analyzing the results. Part 2 will contain results from extensive aging studies of fibercomposite dowels and reinforcing bars cast in a concrete specimen.

The aging test specimens are undergoing accelerated aging at the time of this report (Part 1). Part 2 of the final report will be submitted subsequently.

Abstract

The feasibility of substituting fibercomposite (FC) (thermoset) pavement dowels for steel pavement dowels was investigated in this research project. Load transfer capacity, flexural capacity, and material properties were examined. The objectives of Part 1 of this final report included the shear behavior and strength deformations of FC dowel bars without aging. Part 2 will contain the aging effects. This model included the effects of modulus of elasticity for the pavement dowel and concrete, dowel diameter, subgrade stiffness, and concrete compressive strength.

An experimental investigation was carried out to establish the modulus of dowel support which is an important parameter for the analysis of dowels. The experimental investigation included measured deflections, observed behavioral characteristics, and failure mode observations. An extensive study was performed on various shear testing procedures. A modified Iosipescu shear method was selected for the test procedure. Also, a special test frame was designed and fabricated for this procedure.

The experimental values of modulus of support for shear and FC dowels were used for arriving at the critical stresses and deflections for the theoretical model developed. Different theoretical methods based on analyses suggested by Timoshenko, Friberg, Bradbury, and Westergaard were studied and a comprehensive theoretical model was developed.

The fibercomposite dowels were found to provide strengths and behavioral characteristics that appear promising as a potential substitute for steel dowels.

iv

Table of Contents

List of Symbols

A,B,C,D	constants used to represent the solution for deflection of dowel
A_d	area of the dowel (in^2)
a	radius of circular contact area of load (in.)
d	diameter of dowel (in.)
E	modulus of elasticity of pavement concrete (psi)
EI_z	flexural rigidity of dowel (lb-in^2)
F	form factor, equal to 10/9 for solid circular section
G	shear modulus (psi)
I_z	flexural moment of inertia (in^4)
f	bending stress in dowel (psi)
f_c	pressure at the face of the joint (lb/in)
h	thickness of pavement (in.)
K	modulus of foundation (psi)
k	modulus of subgrade reaction (pci)
k_o	modulus of dowel support (pci)
L	length of dowel embedded on one side of the joint (in.)
L_s	shear span of the dowel within the joint opening (in.)
ℓ	total length of dowel bar (in.)
ℓ_r	radius of relative stiffness (in.)
M	bending moment in dowel (lb-in)
M_o	bending moment in dowel at the face of the joint (lb-in)
P	load applied at the edge of pavement slab joint (lb)
P_t	force transferred by the critical dowel (lb)
p	term used to define Bradbury's pressure distribution
Q	first moment of area (in^3)
q	intensity of load acting on the beam (psi)
R	radius of dowel (in.)
S	section modulus of dowel (in^3)
T	torque (lb-in)
t	width of cross section (in.)
V	shear force in dowel (lb)

X	length of dowel on one side of the joint covered by first positive and negative pressure cycles (in.)
x	distance along dowel from the face of the joint (in.)
x_m	point of maximum bending moment on the dowel (in.)
y	deflection of dowel (in.)
y_o	deflection of dowel at the face of the joint (in.)
z	width of joint opening (in.)
μ	poisson's ratio of pavement concrete
β	term used for mathematical expediency (in^{-1})
σ	bearing stress in concrete (psi)
σ_d	contribution to the stress in concrete from dowel reactions (psi)
σ_e	tensile stress produced by edge loading alone (psi)
τ	shearing stress in dowel (psi)
Δ	total relative deflection of two slabs at the joint (in.)
δ	shear deflection of that part of the dowel in joint opening (in.)

Disclaimer

The contents of this report do not represent a warranty of the products used on behalf of the State of Iowa, Iowa State University, Iowa Department of Transportation, Highway Research Board, or the authors. The opinions, findings, and conclusions expressed in this publication are those of the author and not necessarily those of the Highway Division of the Iowa Department of Transportation. Engineering data, design, details, with recognized professional principals and practices are for general information only. The data, designs, and suggested conclusions should not be used without first securing competent advice with respect to the suitability for any given application. The responsibility for the use of information in this report remains with the user. This report is for information purposes and is made available with the understanding that it will not be cited without the permission of the authors.

List of Figures

List of Tables

1.0.   Introduction

1.1.   Needs for Alternative Concrete Reinforcement Materials

A considerable number of the nation's concrete bridges, roads, parking structures and marine structures need repair or replacement because of deterioration resulting from the corrosion of the reinforcement. New construction methods and new materials are needed to protect the infrastructure so this type of deterioration can be avoided in the future. An obvious method of controlling the infrastructures' deterioration is by using materials that can extend their design lives by reducing or eliminating the corrosion of the reinforcement.

In the specific cases of bridges and highways, corrosion of the steel reinforcement used in concrete is a major cause of deterioration [2]. Epoxy-coated steel reinforcement was seen as the cure to this problem, but some reports of the performance of the epoxy-coated steel are less than encouraging [3]. One such report by Kenneth C. Clear states "based on our work to date, it appears obvious that epoxy-coated reinforcing steel can no longer be considered a viable primary protective system" [4:p.61]. For example, in the Florida Keys, bridge piers reinforced with conventional black steel were experiencing corrosion problems. The federal government then set a standard that all piers constructed in this type of environment must use epoxy-coated reinforcement exclusively. The bridge piers constructed with epoxy-coated steel corroded after a relatively short period of time at a very fast rate, even faster than the corrosion rate that occurred to the bridge piers with black reinforcement steel. The reason for the extremely high rate of corrosion in this case is not known at this time, but voids in the coverage of the epoxy on the reinforcement may be setting up a reaction between the exposed metal ions and the salt water. At the location of the void, corrosion would progress at a much faster rate because of the cathode-anode reaction occurring between the protected region of the bar and the void. In this case, the bridge piers had a significantly shorter design life with the epoxy-coated steel than with the ordinary black steel as reinforcement.

Epoxy-coated reinforcing steel can be expected to resist corrosion very effectively if no voids exist in the epoxy coating. Simply moving the bars to stock piles or stacking them on top of each other in the factories where the epoxy is applied can easily nick the coating. Additionally, construction workers commonly nick the coating during the placing of the steel reinforcement. Although careful handling of the bars and repairing of discovered nicks can reduce the number of imperfections in the coating, nicks or pinholes cannot be entirely eliminated. A single nick is all that is required to begin the corrosion process of a reinforcement bar. To expect that epoxy-coated steel bars are free of corrosion

problems is far from practical. To avoid corrosion of the reinforcement, a method other than epoxy coating should be used.

A logical choice is to use a material which is naturally resistant to the corrosive environments that it is placed in, thus eliminating the possibility of corrosion. Fibercomposites are a material expected to be naturally corrosion resistant, and they may prove to be more corrosion resistant than epoxy-coated steel. Steel and fibercomposite bars do not corrode in a similar manner because they are not affected by the same types of corrosive agents.

1.2. Background on Fibercomposites

Fibercomposites are a class of materials composed of a combination of fibers and resin. Although there are many possible applications of fibercomposite materials, to date, most are of a specialty or exotic nature. Most of the applications for fibercomposites presently are in the aerospace and aeronautics industries. The space shuttles, stealth fighters and bombers, and the B-1 bomber are some of the aircraft made in part from fibercomposites [5]. Some other well known applications for fibercomposites are car body panels, boats, tennis and racquetball rackets, and fishing poles [6].

Fibercomposites are made in many shapes and forms. Mats, resin combined with alternating angled layers of parallel fibers, are a common form of fibercomposites. Rod stock, parallel fibers combined with a resin, are being researched as an alternative to steel reinforcement bars. In addition, W-shapes, channels, angles, square bars, round bars, and tubes are other commonly stocked cross sections carried by some manufacturers.

To date, the use of fibercomposites in structural applications is very limited. Unfamiliarity with the benefits of fibercomposites, a general lack of information on their design procedures, skepticism associated with the use of a new material, and concerns over the behavior and failure methods of structures using these materials have kept most structural engineers from utilizing fibercomposite materials in their designs. However, research is currently being conducted at several universities [7,8] that will aid in explaining the behavior of various structures utilizing fibercomposite materials.

The research into fibercomposites is expanding, and as a result, technological advances in material properties are being developed rapidly [9]. More refined design procedures for structural applications of fibercomposite materials are expected to be developed in the near future. The development of new design procedures and the research to support them should make fibercomposite materials more appealing to structural engineers.

Fibercomposites have some advantages in structural applications, as well as some disadvantages. Some of the advantageous characteristics of fibercomposite materials include [10]:

1) Very high corrosion resistance,
2) High tensile strength,
3) High strength-to-weight ratio,
4) Good thermal insulation properties,
5) High electrical resistance (low conductivity) properties,
6) Competitive cost with standard construction materials,
7) Architectural appearance easily controlled with the use of different colored resins, and
8) Good fatigue behavior.

Fibercomposite materials also have some significant disadvantages [10]:

1) Low modulus of elasticity,
2) Brittle failures,
3) Material shape unalterable (i.e., cannot be bent) after initial manufacture for thermoset resins,
4) Anisotropic material behavior,
5) Material's creep behavior unknown,
6) Poor bond characteristics, compared to steel, due to the difficulty manufacturing deformed FC bars,
7) Generally poor fire resistance, and
8) Relatively low shear strengths.

Bars made of parallel fibers, instead of steel, have recently been used by some structural engineers as reinforcement in concrete. Fibercomposite concrete reinforcing bars generally have higher tensile strengths, much higher resistance to corrosion, much lower thermal and electrical conductivities, and much lower weights than steel reinforcement bars [11].

The advantageous properties of the fibercomposites have sparked an interest in many areas of construction that could benefit by these characteristics. Higher corrosion, electrical and thermal resistance can benefit some types of structures.

Higher electrical resistance can be important in some instances. For example, some hospitals have equipment that is very sensitive to outside electrical currents [12]. Currents can be induced in the building's steel reinforcement if the reinforcement is exposed to large magnetic fields. Fibercomposite reinforcement, on the other hand, has a much higher electrical resistance to these types of fields and may reduce the induced current down to an acceptable level [13]. Fibercomposite reinforcement had been successfully used in the construction of Medical Center Hospital, San Antonio, Texas [14].

Fibercomposite's higher thermal resistance can also be an important factor. Concrete sandwich panels made from layers of concrete and insulation connected with fibercomposite ties instead of steel ties can significantly reduce thermal losses [15].

The higher corrosion resistance of fibercomposites is significant in pavement joint dowels, bridges, piers and other structures where corrosion of the reinforcement is a major problem. Many of these structures could benefit from the use of highly corrosion resistant fibercomposite reinforcing bars.

There are many other examples of structures that can benefit from the use of fibercomposites. The above examples are merely a few of the possible applications for this material.

1.3. Research Program

In spite of the advantages of fibercomposite (FC) reinforcing bars (rebars) over steel, some design characteristics of the behavior of FC need to be determined for examining the feasibility of FC dowels and reinforcing bars in concrete pavement and bridges. The objective of this research project was aimed at determining the aging and degradation effects on shear behavior of FC dowels and bond behavior of FC reinforcing bars.

The investigation described herein was conducted at Iowa State University (ISU) in coordination with the Iowa Department of Transportation (IDOT). This work was conducted at the ISU Structural Engineering Laboratory under the auspices of the Engineering Research Institute (ERI) with funds provided by IDOT.

1.3.1. Objective

The objectives of this research project were to determine the following:
1. Shear behavior and strength of FC dowel bars without aging,
2. Shear behavior and strength of FC dowel bars with aging,
3. Potential aging effects on bond of FC reinforcing bars.

1.3.2. Scope

The scope of this research project included:

1. Selecting an appropriate theoretical model for analyzing the results,
2. Design and construction of experimental tests for

Objectives 1 and 2,

3. Testing the dowel-shear specimens both aged and unaged,
4. Analyzing the dowel shear testing results,
5. Design and construction of the test specimen details for examining the aging effects on bond behavior of FC reinforcing bars in concrete,
6. Conduct experiments and analyze results for FC reinforcing bars.

1.4. Literature Review

The Literature Review encompassed FC materials, pavement dowels, shear testing, and aging. A complete discussion of the appropriate references can be found in the sections most closely associated with the topic.

2.0. Analysis of Pavement Dowels

2.1. Introduction

The load transfer capacity of a dowel bar is the maximum load that the bar can transfer across the joint as limited by the following failure modes: shear on the bar, bending in the bar, bearing or crushing of the concrete, splitting the underneath wedged shaped portion of concrete, or a combination of these modes. The purpose of the analysis of dowels is to find the critical stresses associated with these failure modes. When a load is applied to the edge of the joint on one of the slabs (refer to Figure 2.1), some portion of the load is transferred to the subgrade. The remaining load is transferred to the unloaded slab through the dowels. The dowel which is nearest to the applied load is the more highly stressed dowel because it transfers a higher portion of the load. The shear force carried by the more highly stressed dowel can be determined by assuming a linear distribution of the transferred load among the dowels as explained in Section 2.1.2. The more highly stressed dowel can then be analyzed for critical stresses by using one of the theoretical models presented in Section 2.1.3.
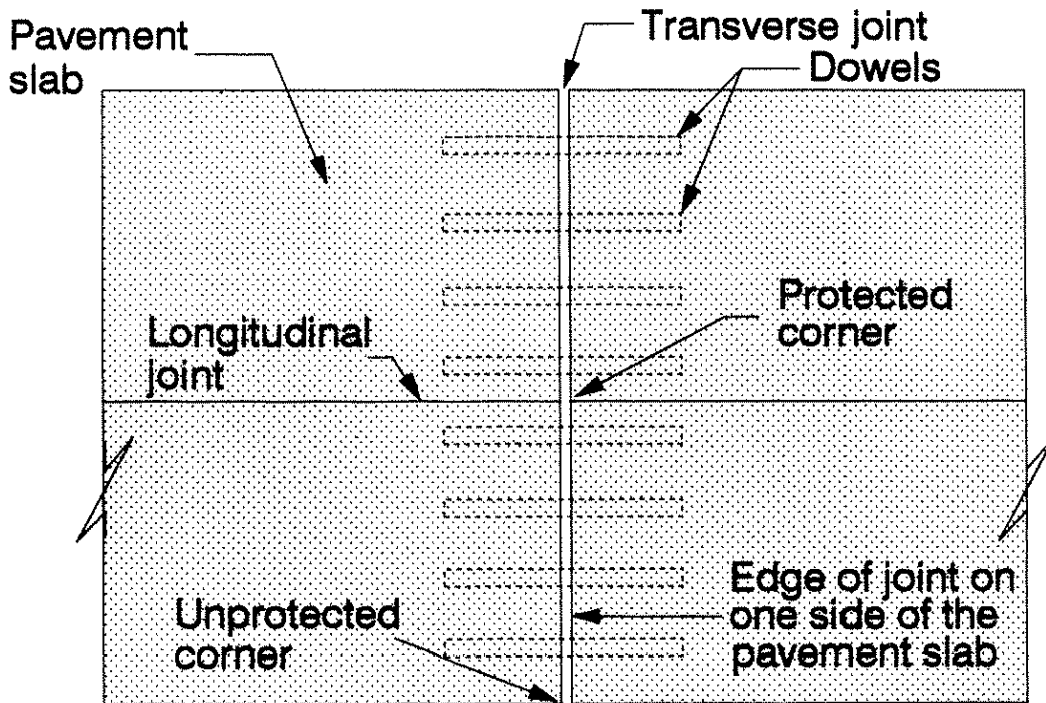
Figure 2.1. Schematic showing top view of pavement slab

2.1.1. Load transfer

Pavement dowels are installed at a transverse joint for establishing load transfer across the joint. The purpose of providing the load transfer is to reduce the deflections and edge stresses at a joint and therefore the load transfer is a direct measure of the effectiveness of dowel bars. If the dowels are assumed to be perfectly rigid so that each slab at the joint deflects by an equal amount, then half of the load applied on one slab will be transferred to the unloaded slab through dowels [16]. A reduction in load transfer due to the dowel looseness resulting from the action of repeated loads can be assumed to be about 5 to 10 percent. Therefore the design load transfer should be taken as 45 percent of the design load [17].

2.1.2. Distribution of transferred load

When a load is applied at a joint, the dowel bars which are under or nearest to the point of application of load assume a higher portion of the transferred load with the shear carried by the dowels being decreased progressively with the distance from the load. Friberg [18] suggested that only the dowels contained within a distance of $1.8\ell_r$ from the load are active in transferring the load where ℓ_r is the radius of relative stiffness, defined by Westergaard [19] as follows:

$$\ell_r = \sqrt[4]{\frac{Eh^3}{12(1-\mu^2)k}} \qquad \text{Eqn. 2.1}$$

where:
ℓ_r = radius of relative stiffness (in.)
E = modulus of elasticity of the pavement concrete (psi)
h = thickness of the pavement (in.)
μ = poisson's ratio
k = modulus of subgrade reaction (pci).

The load transferred across the joint is assumed to be distributed linearly among the dowels contained within an effective length of $1.8\ell_r$ from the load. If the load transferred through the dowel nearest to the applied load is denoted by P_t then distribution of shear forces carried by the active dowels expressed in terms of P_t is as shown in Figure 2.2a. To determine the dowel shears under the action of two or more loads, superposition of effects of individual loads can be adopted.

Tabatabie, et al [20,21] made use of a finite element model for pavement joint analysis and suggested that only the dowels within $1.0\ell_r$ from the center of the load are active [22]. Tabatabie proposed a linear approximation to the distribution of dowel shears as shown in Figure 2.2b.
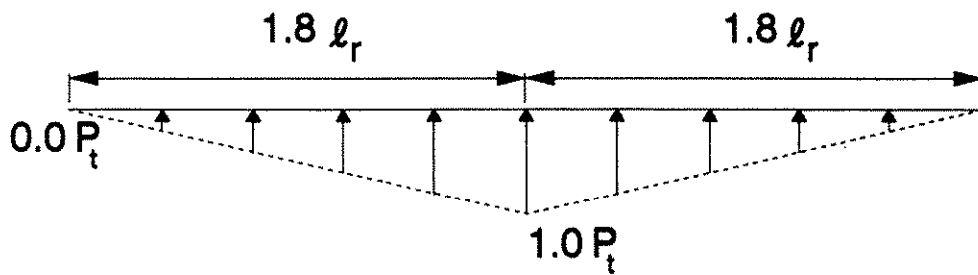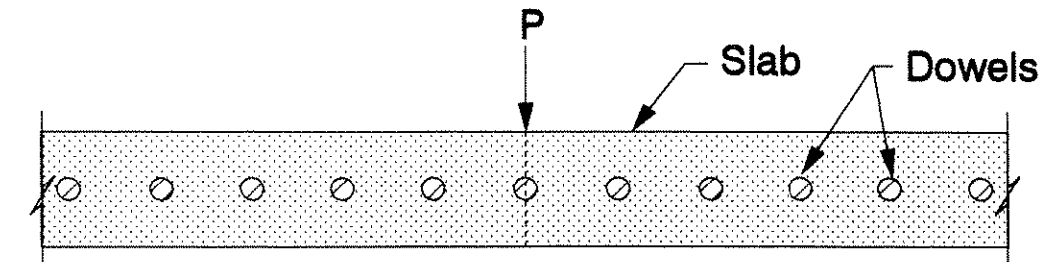
a. Effective length of 1.8 ℓ_r
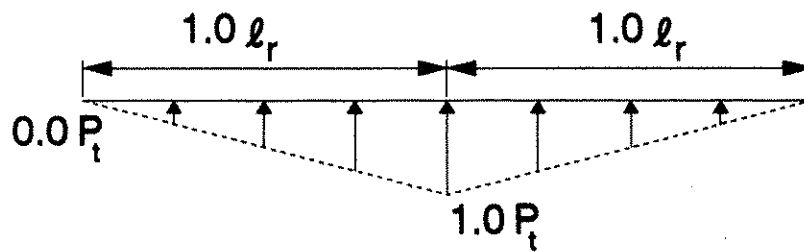
b. Effective length of 1.0 ℓ_r

Figure 2.2. Schematic of load over the effective number of dowels

Distribution of shear force depends on the location of the load, i.e. whether the load is applied on an edge, protected corner, or unprotected corner (see Figure 2.1). Friberg, however, considered only the edge loading for arriving at the effective length of $1.8\ell_r$. The effective length will be shorter for corner loading than that for the edge loading. Also, a decrease in effective length increases the intensity of stress and therefore adoption of a shorter effective length is conservative. Because of the above reasons, an effective length of $1.0\ell_r$ is recommended by Tabatabie [22].

2.1.3. Determination of critical stresses

Once the magnitude of transferred load, and subsequently the distribution of shear among the dowels is determined, the bearing stress on the concrete, bending stress in the bar, and the shearing stress on the bar can be determined for the more highly stressed dowel by using a theoretical model for idealizing the dowel-concrete system. If the shear transferred by the critical dowel is P_t and the joint width is designated as z, then the external forces acting on that part of the dowel extending across the joint opening are as shown in Figure 2.3. Equilibrium of this element requires that $M_1 + M_2 = P_t z$. If the dowel has the same condition of embedment in each slab, then one can assume that $M_1 = M_2$. The bending moment at either face of the joint can then be obtained as follows [23]:

$$M_1 = \frac{P_t z}{2} = -M_o$$

Eqn. 2.2

where M_o is the moment in the dowel bar at the face of the joint, taken as positive when acting clockwise. Also, since the concrete is very stiff compared to the dowel, a point of contraflexure can be assumed in the dowel at the center of the joint. In this case the above expression for the moment in the dowel at the face of the joint is acceptable [18].

For analysis purposes, only that part of the dowel bar embedded on one side of the joint may be idealized as a beam encased in an elastic medium, being acted upon by the shear P_t and the moment M_o as in Figure 2.4. The dowel bar can then be analyzed for critical stresses by employing the analysis procedures discussed in the following section.
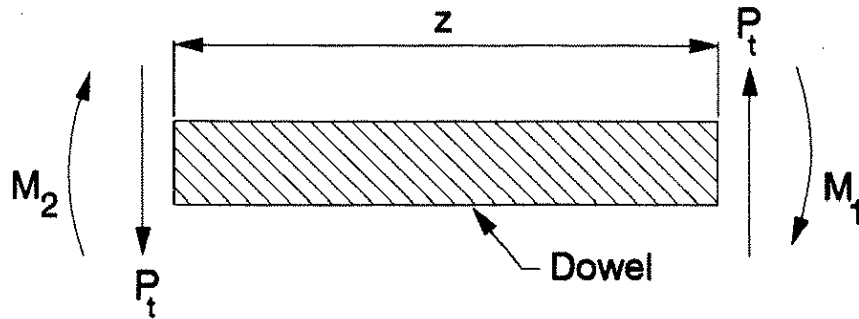
Figure 2.3. Equilibrium of portion of the dowel extending across the joint opening
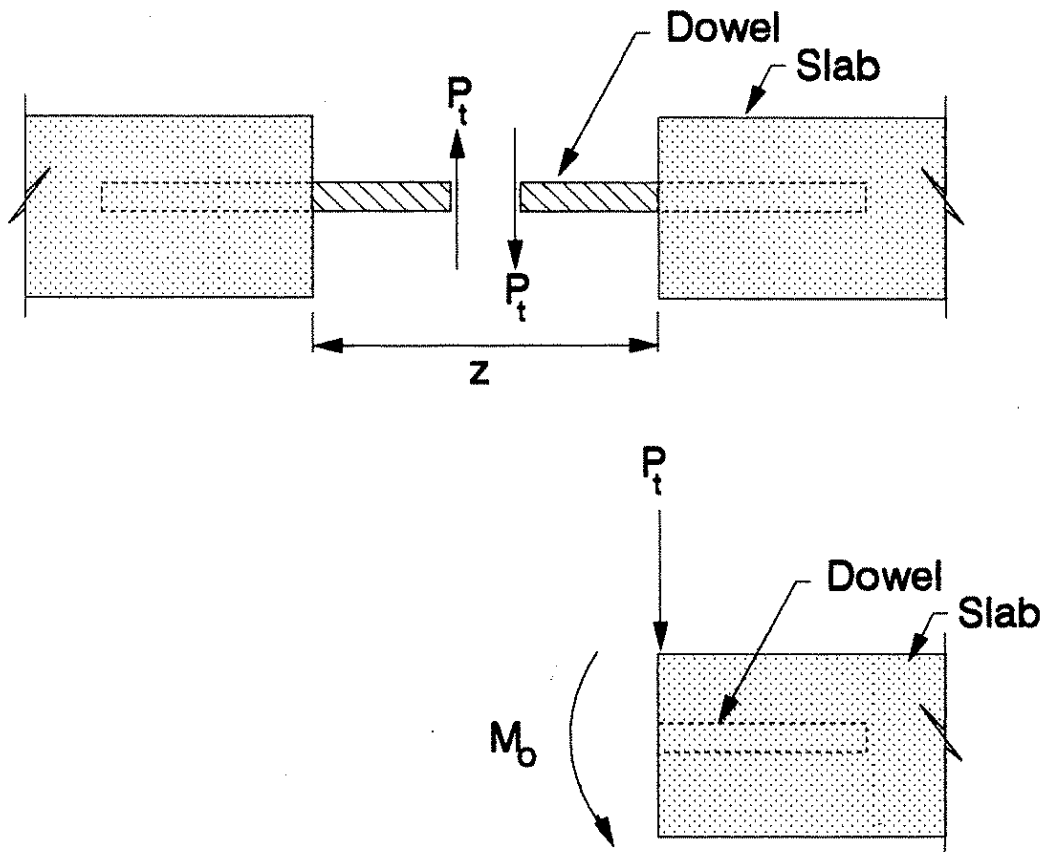

Figure 2.4. Pavement as a beam encased in an elastic medium

2.2. Theoretical Models

Four different theoretical methods developed by Timoshenko, Friberg, Bradbury and Westergaard were investigated. Timoshenko's analysis was found to be the most appropriate for the analysis of pavement dowels.   A description of Timoshenko's analysis is presented along with a brief discussion on the other three methods with respect to the rationale for following Timoshenko's analysis.

2.2.1. Analysis based on Timoshenko's theory

Timoshenko, in his analysis of beams on elastic foundation [24,25] considers the following three cases:

(i)   Infinite beams: Beams extending to infinity on either side of the origin fall under this class (Figure 2.5a).

(ii)   Semi-infinite beams: Those with one end located at the origin and the other extending to infinity are semi-infinite beams (Figure 2.5b).

(iii) Finite beams: These are the beams with both the ends located at finite points, or in other words beams of finite length (Figure 2.5c).

Timoshenko introduces a constant K, called the modulus of foundation, which denotes the reaction per unit length when the deflection is unity. This factor assumes that when the beam is deflected, the intensity of continuously distributed reaction at every point is directly proportional to the deflection at that point. The differential equation for deflection of the beam can be written as:

$$EI_z \frac{d^4 y}{dx^4} = q$$

Eqn. 2.3

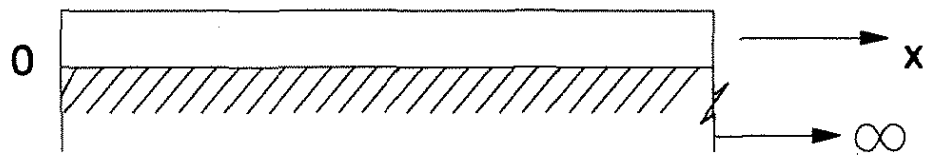where q is the intensity of the load acting on the beam which, for the unloaded portion of the beam is equal to -Ky. Equation 2.3 can then be written as shown in Equation 2.4.
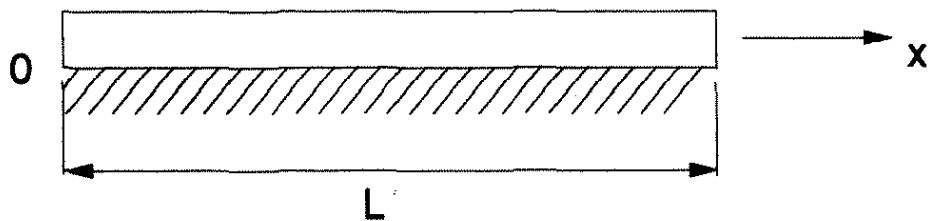
$$EI_z \frac{d^4 y}{dx^4} = -Ky$$

Eqn. 2.4

Timoshenko presents the general solution which is applicable to all the cases of beams as follows:
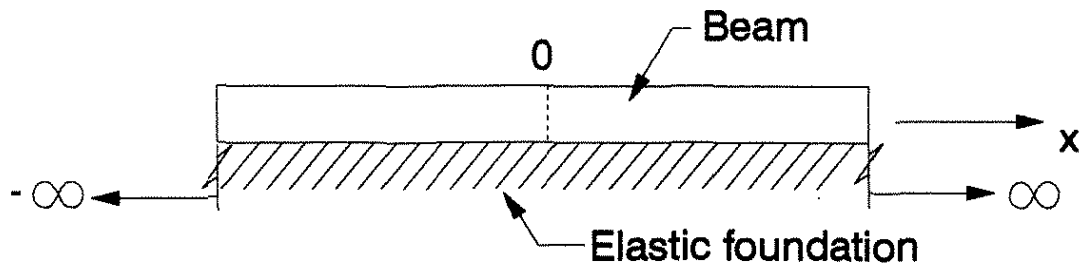
a. Infinite beam

b. Semi-infinite beam

c. Finite beam

Figure 2.5. Beams on elastic foundation

$$y = e^{\beta x}(A\cos\beta x + B\sin\beta x) + e^{-\beta x}(C\cos\beta x + D\sin\beta x) \qquad \text{Eqn. 2.5}$$

where:

$$\beta = \sqrt[4]{\frac{K}{4EI_z}} \ (in.^{-1})$$

K = modulus of foundation (psi)
EI_z = flexural rigidity of the beam (lb-in²).

The constants A, B, C and D can be found by applying the appropriate boundary conditions. Once these constants are determined, the equation for deflection along the length of the beam can be established. Furthermore, by differentiating the deflection equation successively, one can find the distribution of bending moment, shear force and pressure along the beam. These equations are of sinusoidal form with rapidly decreasing amplitude along the length of the dowel.

For the analysis of a pavement dowel, the problem can be idealized as a finite beam resting on an elastic foundation as shown in Figure 2.6 where L is the embedded length of the dowel on one side of the joint. The effect of the action of forces, applied at one end of the beam, on the deflection at the other end depends on the magnitude of the quantity ß times the length, L. This can be observed from the solution of the finite beam problem. Beyond a certain value of ßL, a force acting at one end of the beam has only a negligible effect at the other end in which case, one can consider the beam to be an infinitely long beam. In such cases, the dowel-concrete system may be idealized as a semi-infinite beam resting on an elastic foundation with one of its ends being at the origin and the other at infinity. Applying the boundary conditions with respect to the forces acting at the origin and forcing the deflection and bending moment to be zero at infinity, one can obtain the solution for the semi-infinite case as follows:

$$y = \frac{e^{-\beta x}}{2\beta^3 EI_z} [P_t\cos\beta x - \beta M_o(\cos\beta x - \sin\beta x)] \qquad \text{Eqn. 2.6}$$

where:
P_t = force (shear transferred by the dowel) (lb)
M_o = moment acting at the end held at the origin (lb-in).

When the pavement dowel is idealized as a semi-infinite beam, the solution may result in residual bending moment and shear force at the end of the dowel. However, these values may approach zero as the magnitude of ßL increases. Timoshenko presents a general classification of finite beams as follows:
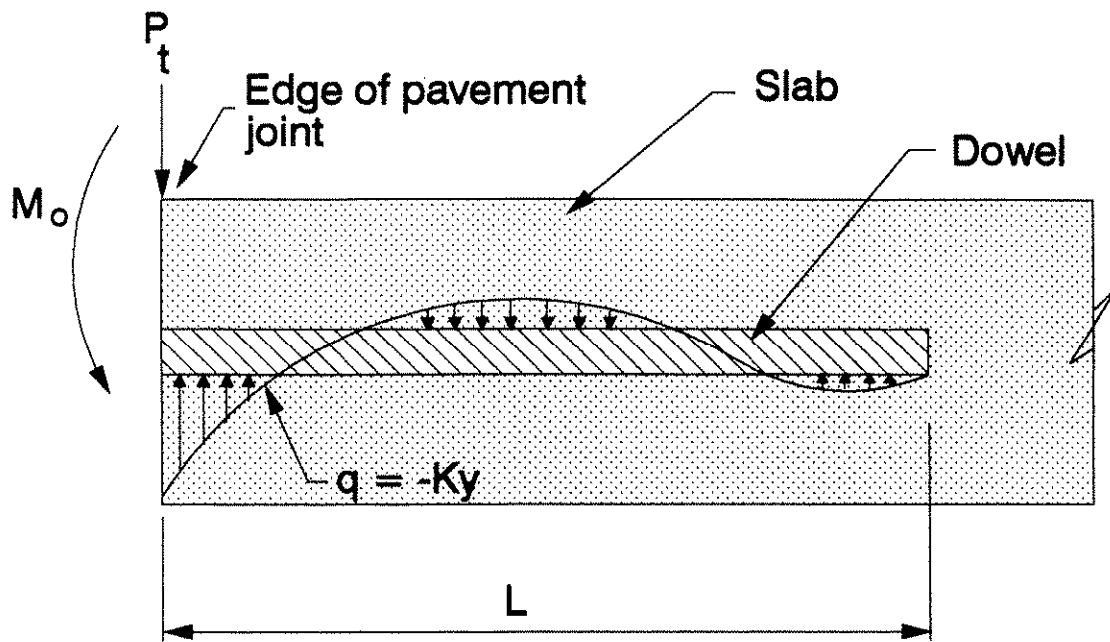
Figure 2.6. Finite beam idealization of dowel concrete system

(i)   short beams: $\beta L < 0.6$
(ii)   beams of medium length: $0.6 < \beta L < 5$
(iii) long beams: $\beta L > 5$

Beams of group (i) can be assumed to be very rigid and the deflection due to bending may be entirely neglected. Practical cases of pavement dowels fall under either group (ii) or (iii). The characterizing parameter of beams in group (ii) is that a force acting at one end of the beam produces a considerable effect on the other end and hence such beams must be treated as beams of finite length. The beams of group (iii) can be treated as beams of infinite length.

Thus, for cases where $\beta L < 5$, the dowel should be treated as a beam of finite length and the exact solution to the finite beam problem should be sought by applying the actual boundary conditions at the ends of the dowel to the general solution (Equation 2.5) for beams on elastic foundation. The solution of a finite beam problem is explained later in Section 2.3.2.

2.2.2. Analysis based on Friberg's theoretical model

Friberg [18] adopted Timoshenko's solution given by Equation 2.6 for a semi-infinite beam resting on an elastic foundation as the basis for the analysis of pavement dowels. Substituting x=0 in Equation 2.6, the deflection of the dowel, y_o at the face of the joint can be obtained as in Equation 2.7.

$$y_o = \frac{P_t(2+\beta z)}{4\beta^3 EI_z} \qquad\qquad \text{Eqn. 2.7}$$

where:

$$\beta = \sqrt[4]{\frac{k_o d}{4EI_z}}$$

k_o = modulus of dowel support (pci)
d = diameter of the dowel (in.)

The modulus of dowel support, k_o is the reaction per unit area causing a unit deflection. Since Timoshenko's modulus of foundation is the reaction per unit length causing a unit deflection, we have

$$K = k_o d \qquad\qquad \text{Eqn. 2.8}$$

and therefore the expressions for β as suggested by Timoshenko and Friberg are essentially the same. The bearing pressure on the concrete at the face of the joint is obtained as shown in Equation 2.9.

$$\sigma = k_o y_o \qquad\qquad \text{Eqn. 2.9}$$

By successive differentiation of Equation 2.6, expressions for the bending moment and shear force can be obtained as given in Equations 2.10 and 2.11.

$$M = -EI_z \frac{d^2 y}{dx^2} = -\frac{e^{-\beta x}}{\beta} [P_t \sin\beta x - \beta M_o (\sin\beta x + \cos\beta x)] \qquad \text{Eqn. 2.10}$$

$$V = \frac{dM}{dx} = -e^{-\beta x} [(2\beta M_o - P_t) \sin\beta x + P_t \cos\beta x] \qquad \text{Eqn. 2.11}$$

By equating the shear force to zero, the point of zero shear can be found from Equation 2.11. Evaluation of the bending moment at this point using Equation 2.10 yields the maximum bending moment in the dowel as shown in Equation 2.12.

$$M_{max} = -\frac{P_t e^{-\beta x_m}}{2\beta} \sqrt{1 + (1+\beta z)^2} \qquad \text{Eqn. 2.12}$$

where:
  x_m is the point of maximum bending moment on the dowel (in.)
 $x_m = \cot (1+\beta z)/\beta$

Equations 2.9 and 2.12 can be directly used for stress computations which are based on the solution for a semi-infinite beam. This may not always be a good approximation. The analysis may give an even poorer approximation for a fiber composite dowel system than for a steel dowel system because the low value of K for fiber composite dowels makes the magnitude of βL smaller. Based on the discussion of βL presented in Section 2.2.1., Friberg's analysis can be adopted only when βL is greater than 5.

2.2.3. Analysis based on Bradbury's theoretical model

Bradbury's [23] theoretical model also is based on Timoshenko's analysis. While attempting to analyze the pavement dowel, Bradbury modified Timoshenko's pressure diagram as shown in Figure 2.7a where X is the length of the dowel bar on one side of the joint covered by the first positive and negative pressure cycles. As is evident from Figure 2.7a, Bradbury considered modifying the pressure diagram corresponding to an infinitely long beam. The reasons for modification, as explained by Bradbury are:
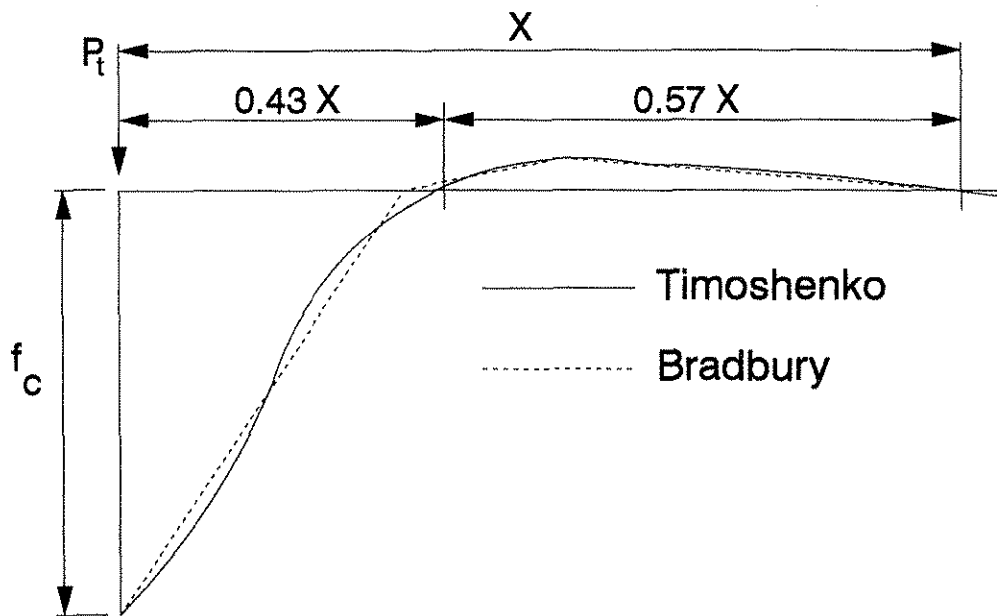
a. Modification of distribution of pressure
on embedded bar of infinite length
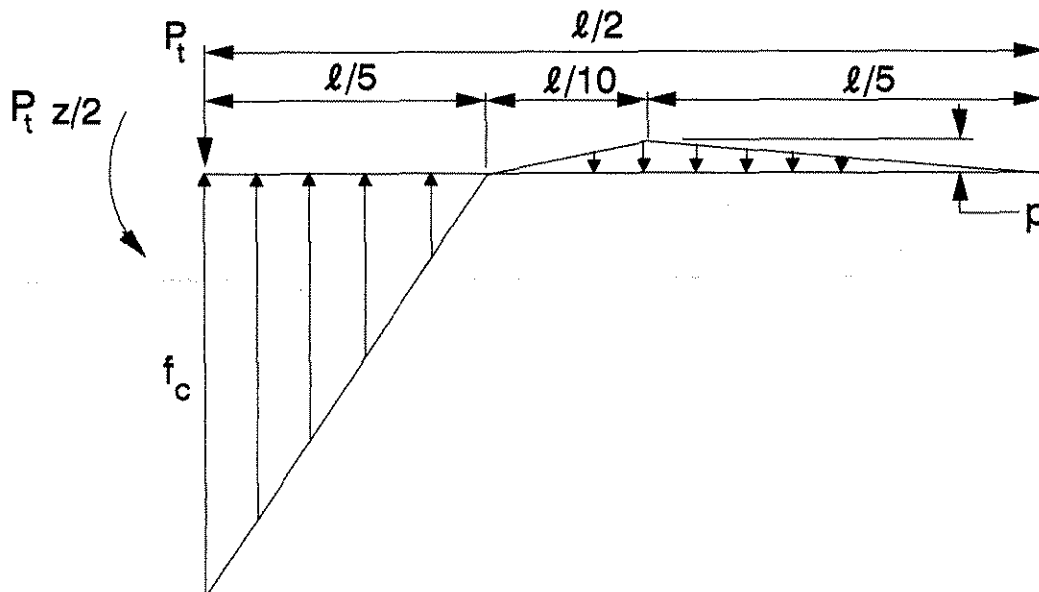
b. Assumed pressure distribution

Figure 2.7. Bradbury's modification to Timoshenko's
pressure distribution

(i)   Pavement dowel is finite, rather than, infinite in length.

(ii)   The modulus of foundation for a dowel is not readily available for evaluation because the slab itself is being supported by a yielding material, i.e. subgrade.

(iii)   The modified pressure diagram, which is in the form of a series of linear loads as shown in Figure 2.7b permits the analysis to be carried out by statics.

Assuming that X is approximately equal to half the dowel bar length, and applying equilibrium conditions, the peak values in Figure 2.7b can be obtained as follows:

$$p = \frac{5P_t(\ell + 7.5z)}{3\ell^2 d} \qquad \text{Eqn. 2.13}$$

$$f_c = \frac{25P_t(\ell + 1.5z)}{2\ell^2 d} \qquad \text{Eqn. 2.14}$$

where:
    ℓ = total length of the dowel bar = 2L + z (in.)
    d = diameter of the dowel (in.).

The values of p and f_c completely define the pressure distribution along the dowel. This reduces the problem to an ordinary beam loaded with linear loads which can be easily analyzed for the required stresses.

Bradbury's analysis is independent of K which is an important variable in the analysis of dowels. Modification of the pressure diagram is not necessary to yield a simplified model because even the accurate solution for the finite beam problem involves solving four simultaneous equations (as will be shown later in Section 2.3.2). Solving these four simultaneous equations is very practical in light of the wide availability of powerful computers.

2.2.4. Analysis based on Westergaard's theory

Westergaard [19] investigated three cases of loading for computing the critical stresses in concrete pavements: (i) corner load, (ii) interior load, and (iii) edge load. He presented the equation for maximum tensile stress (at the bottom of the slab directly under the applied load) for the edge loading case as given in Equation 2.15, which for $\mu=0.15$ is given by Equation 2.16.

$$\sigma_e = 0.529 (1+0.54\mu) \frac{P}{h^2} [\log_{10}(\frac{Eh^3}{kb^4}) - 0.71] \qquad \text{Eqn. 2.15}$$

$$\sigma_e = 0.572 \frac{P}{h^2} [4\log_{10}(\frac{\ell_r}{b}) + 0.359] \qquad \text{Eqn. 2.16}$$

where:

$b = \sqrt{1.6a^2 + h^2} - 0.625h \ (in.)$

a = radius of circular area of contact of load P (in.)
σ_e = free edge stress, as given by Equation 2.16 (psi)

This expression gives the maximum stress in the slab for the case of free edge loading. The effect of introducing dowels at an edge of a pavement joint is to reduce the bending stress in the concrete. By furthering his theory, Westergaard [16] presented the first rational procedure for computing the stresses for a doweled joint.

Assuming that the deflection of loaded and unloaded slabs at a joint is symmetric about the line at the applied load perpendicular to the edge, the force transferred by any dowel, as a fraction of the applied edge load, can be expressed in terms of the deflections of the slab. Deflections and moments caused by an edge load can be directly obtained from the diagrams developed by Westergaard [19]. Once the dowel reactions are computed from the slab deflections, bending moments produced by dowel reactions can be determined from the moment coefficient diagram. These moments can be used to determine the bending stresses. The resultant tensile stress produced at the bottom of the slab directly under the load is given by [16] Equation 2.17.

$$\sigma = \sigma_e + \sigma_d \qquad \text{Eqn. 2.17}$$

where:

σ_d = contribution from dowel reactions (psi)

Westergaard's analysis does not pay attention to the stiffness of the dowel relative to the concrete. Also, bending stress in the dowel can not be found by Westergaard's method. The analysis does not account for the dowel parameters except that the dowel is assumed to be perfectly rigid, which is not the case.

2.3. Selected Analytical Model for ISU Work

2.3.1. Description

The pavement dowel has been idealized as a beam of finite length encased in an elastic medium. The analytical model used for

the research program was based on Timoshenko's theory for beams on elastic foundations. The modulus of dowel support, k_o has been selected as the key variable defining the dowel-concrete system instead of the modulus of foundation, K, as suggested by Timoshenko. Consequently, Friberg's expression for ß has been used throughout the analysis. The values of k_o for steel and FC dowels were established through experimentation. The analysis was carried out as explained in the following section.

2.3.2. Solution of finite beam problem

The solution of a finite beam resting on an elastic foundation can be obtained by considering Timoshenko's general solution as given by Equation 2.5, and then by applying the appropriate boundary conditions. Successive differentiation of Equation 2.5 yields the following differentials shown in Equations 2.18 and 2.19.

$$\frac{d^2y}{dx^2} = \beta^2 e^{\beta x}[-2A\sin\beta x + 2B\cos\beta x] + \beta^2 e^{-\beta x}[2C\sin\beta x - 2D\cos\beta x] \qquad \text{Eqn. 2.18}$$

$$\frac{d^3y}{dx^3} = 2\beta^3 e^{\beta x}[-A(\cos\beta x + \sin\beta x) + B(\cos\beta x - \sin\beta x)]$$

$$+ 2\beta^3 e^{-\beta x}[C(\cos\beta x - \sin\beta x) + D(\cos\beta x + \sin\beta x)] \qquad \text{Eqn. 2.19}$$

Referring back to Figure 2.6, the boundary conditions can be expressed as listed below:

     (i)   at x=0, M = EI_z d^2y/dx^2 = $- M_o$

     (ii) at x=0, V = $-EI_z$ d^3y/dx^3 = $- P_t$

     (iii) at x=L, M = EI_z d^2y/dx^2 = 0

     (iv) at x=L, V = $-EI_z$ d^3y/dx^3 = 0.

By applying the boundary conditions (i) and (iii) to Equation 2.18, and the boundary conditions (ii) and (iv) to Equation 2.19, a set of four simultaneous equations can be formed. These equations can be solved for the unknowns A, B, C and D. The equations when formed, can be written as:

$$a_{11} A + a_{12} B + a_{13} C + a_{14} D = b_1$$

$$a_{21} A + a_{22} B + a_{23} C + a_{24} D = b_2$$

$$a_{31} A + a_{32} B + a_{33} C + a_{34} D = b_3$$

$$a_{41} A + a_{42} B + a_{43} C + a_{44} D = b_4.$$

Expressing in matrix form,

$$[a] \{A\} = \{b\}$$

$$\text{or } \{A\} = [a]^{-1}\{b\}.$$

Thus, by inverting the matrix [a] and multiplying with {b}, the unknown set {A} can be determined. With the values of A, B, C and D, one can establish the equation for deflection along the dowel. The distribution of bending moment and shear force along the length of the dowel can be derived by differentiating the equation for deflection (or by using Equations 2.18 and 2.19).

2.4. Importance of Experimentation

The modulus of dowel support is a very important term in the analysis of pavement dowels. The value of k_o can not be easily established theoretically. There is no information available as to what value of k_o is to be used in the analysis of specific situations. So, the value of k_o is established through experimentation. The purpose of conducting experiments is to find the maximum deflection, y_o, of the dowel relative to concrete at the face of the joint. The value of y_o will be used to read the value of k_o from a graph relating k_o and y_o. The graph can be theoretically developed by determining a relationship between k_o and y_o by substituting x=0 in deflection equation.

3.0. Experimental Investigation

3.1. Introduction

The investigation described herein (Section 3.0.) was conducted at ISU in coordination with the Iowa Department of Transportation (IDOT). This report covers Objective 1 given in Section 1.3.1, which focused on shear behavior and strength of FC dowel bars without aging.

This experimental investigation discusses the different shear test methods that are available to determine the shear capacity of the dowel bars (Section 3.5.1.), and explains the shear test method chosen for ISU work. The experimental results are discussed in Section 3.6 with load-deflection curves given in Appendix A.

3.2. Objective

The objective (for Part 1 of the final report) focused on a direct comparison between fiber composite (FC) dowel bars and steel dowel bars. Dowel-specimen types included FC dowels from Supplier A and steel dowels. The objective of the dowel testing portion was to determine the suitability of substituting FC dowel bars for steel pavement dowels, which are currently used in practice.

3.3. Scope

The scope of the research included experimental testing of 10-dowel specimens (including five specimens, containing FC dowels from Supplier A, and five-steel dowel specimens) subjected to direct shear. A second FC dowel bar, from Supplier B, was tested and determined as inappropriate for use in this research program. Supplier B FC dowel bars contained surface deformations resulting in considerable bond between the dowel and the concrete (the dowel must not bond to the concrete, which would inhibit expansion and contraction of the pavement slab). Also, Supplier B FC dowel bars had a significantly lower load carrying capacity. The test matrix for the 10 dowel-shear specimens was developed by ISU in coordination with the IDOT and can be found in Table 3.1. Table 3.1 shows the dowel type, the supplier designation and the number of test specimens for the dowel-shear tests.

Table 3.1. Test matrix

Dowel Type	Supplier	Number of Test Specimens
		Unaged (air)
FC	A	5
Steel	O	5

3.4. Materials and Specimens

Dowel-shear specimens were constructed as shown in Figure 3.1. The specimens used in the research program for the dowel-shear tests consisted of a 10- by 10- by 24-inch concrete member with a pavement dowel centered in the concrete. The 10-inch-thick dimension was chosen to represent a commonly used 10-inch-thick pavement. To eliminate problems with handling and testing of the specimens, minimum sizes were used (ie., specimens with 10-inch width). A gap in the specimen (see Figure 3.1) helped insure that no force was transferred by aggregate interlock or interface friction, and that all of the force was transferred through the dowel being tested. To keep the specimen close to field conditions a gap of approximately one-eighth inch was provided.
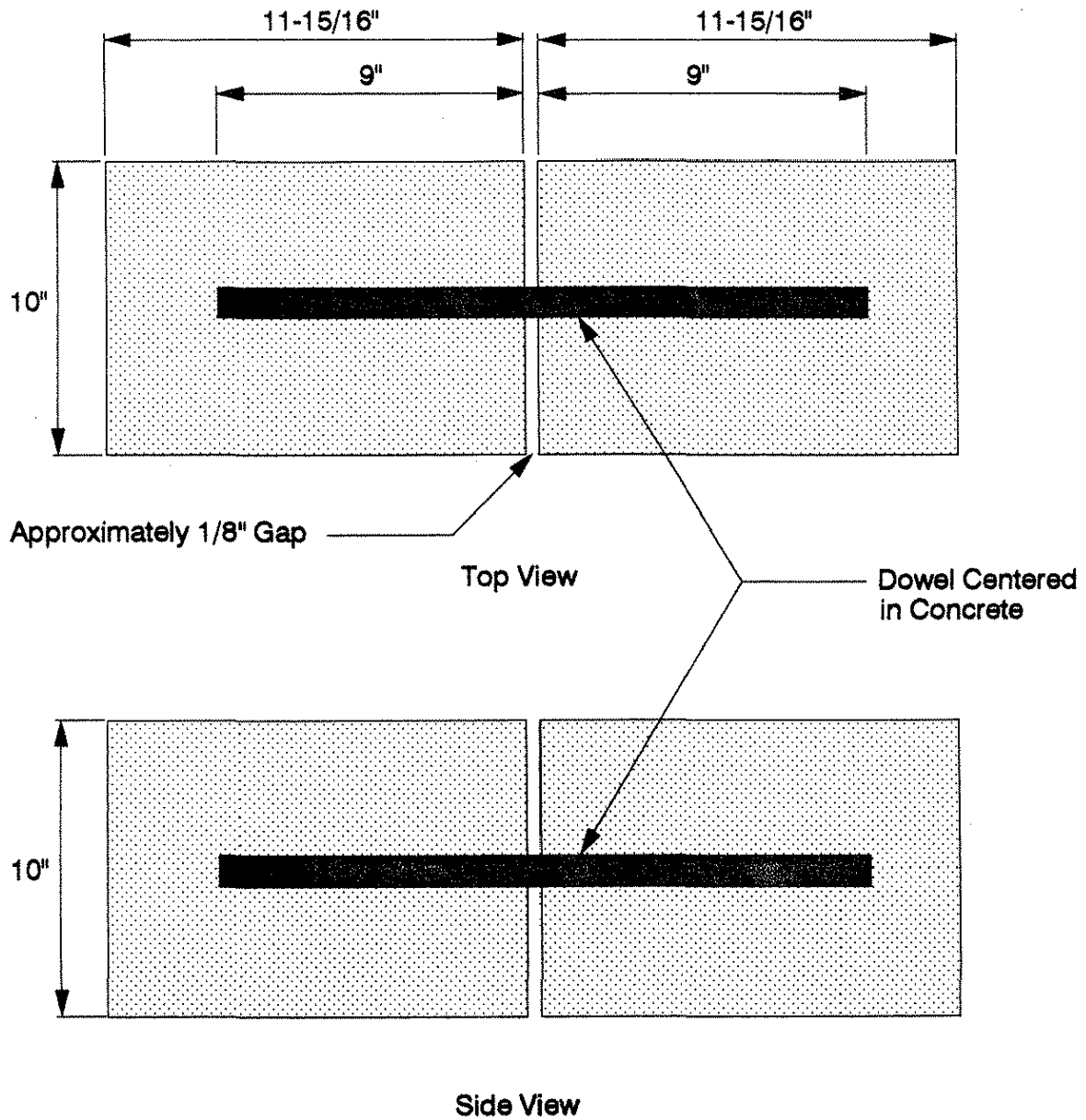
The specimens were constructed with steel prefabricated forms. Three sheet metal pieces were placed at the centerline of each dowel specimen to create the gap. The concrete used was the Iowa Department of Transportation's M-4 mix with superplasticizer. The mix was provided by a local manufacturer. The average strength of the concrete was 8000 psi and was determined based on testing standard cylinders. Table 3.2 lists the properties of the FC and steel dowels used in this investigation.

Table 3.2. FC and steel properties

Dowel Type	Supplier	Dowel Length (in.)	Measured Diameter (in.)	Area (in²)	Apparent Modulus of Elasticity (psi)
FC	A	18	1.250	1.227	2.80×10^{6}[*]
Steel	O	18	1.500	1.767	28.0×10^{6}[**]

[*]   Supplied by manufacturer
[**]   Value was determined through flexural testing

11-15/16"   11-15/16"

9"   9"

10"

Approximately 1/8" Gap

Top View

Dowel Centered
in Concrete

10"

Side View

FC and Steel Assemblies

Figure 3.1. Dowel specimens

3.5. Testing Procedure

The dowel-shear testing procedure was developed to determine the shear capacity of FC and steel dowel bars embedded in concrete (refer to Figures 3.1).   A shear test method was selected to simulate the actual dowel-shear behavior in a pavement joint.

Due to the size and shape of the test specimens (see Figure 1), several different shear test methods were investigated before choosing the more appropriate method for testing the dowel specimens. Section 3.5.1 describes various shear test methods and their suitability for use in this research project.

3.5.1. Shear test methods

3.5.1.1. Short beam test

The short beam shear test involves a short beam specimen (short beam with 4:1 span to thickness ratio) supported at two points with a concentrated load applied at the center of the specimen [27]. Figure 3.2 illustrates the short beam shear test geometry. The shear stress distribution across the cross section can be determined with the elementary beam theory equation (this does not apply to circular sections) as shown in Equation 3.1.

$$\tau = \frac{VQ}{I_z t}$$

Eqn. 3.1

where:

    τ = Shear stress
    V   = Shear force on a cross section(lbs)
    Q   = First moment of area (in^3)
    t   = Width of the cross section (in.)
    I_z = Flexural moment of inertia (in^4)

Because of the simplicity of the test setup, the short beam test has become a popular test method for determining the shear strength of fibercomposites [28]. The short beam test, when used to test unidirectional fibercomposite materials, usually does not yield interlaminar shear failures [27]. Often the failures of the specimens are associated with stress concentrations caused by the combination of the concentrated load at the center and the concentrated reaction points at the ends of the short beam. These three point loads each cause stress concentrations around them, and the combination of three point loads in one very short beam causes significant stress concentration effects throughout the entire beam, questioning the validity of the test [27]. Many researchers
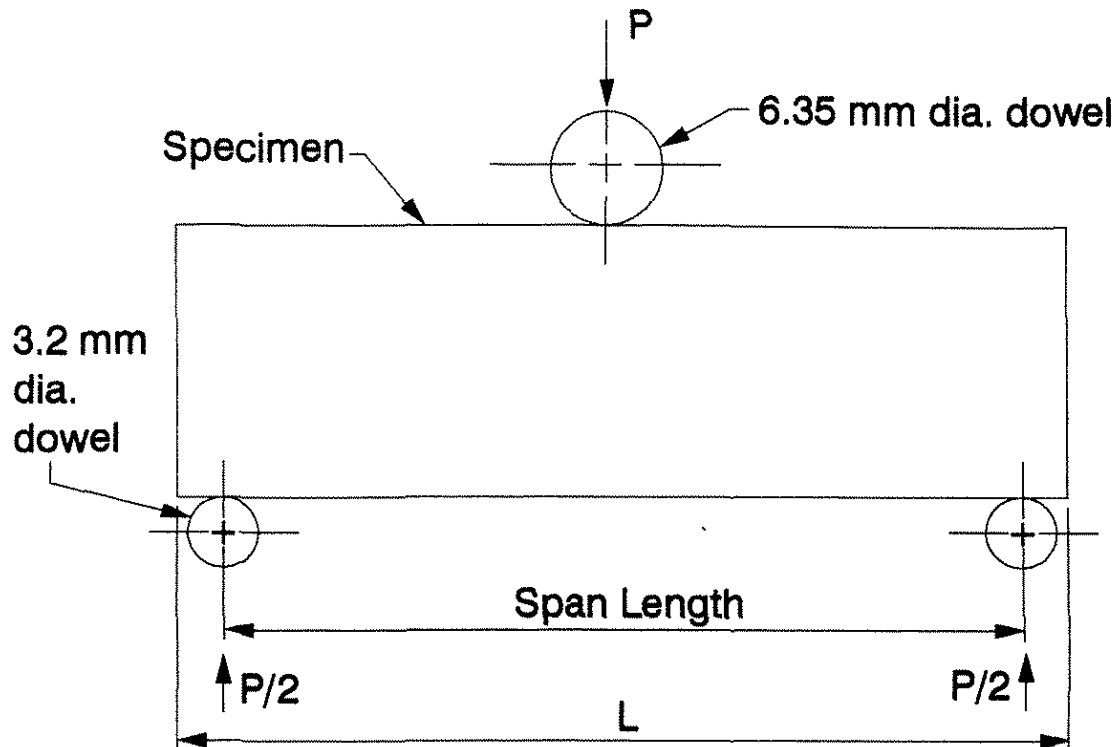
Horizontal Shear Load Diagram
(Flat Laminate)

American Society for Testing and Materials (ASTM)
Recommended Ratio of Support Span to Thickness
and Ratio of Specimen Length to Thickness

Reinforcements	Span/Thickness	Length/Thickness
Glass Fibers	4	7
Graphite Fibers	4	6
Carbon Fibers	4	6
Steel Fibers	4	6

Figure 3.2. Short beam shear test geometry and
specifications (ASTM) [29]

have studied the stress distributions in an anisotropic short beam specimen using a finite element analysis technique [27]. The results from the finite element analysis, verified with photomicrographs of experimental tests, show that the stress concentrations (with resulting maximum stresses on the top fibers up to three times the maximum shear stress on the centerline of the specimen) often can affect the results of the short beam test and that inaccurate results commonly occur while using this test procedure [27].

According to Adams, Thomas, and Rodney the "beam must be relatively short to minimize the possibility of failure in the tensile or compressive mode. Before a shear failure at the neutral axis occurs, the applied concentrated loads become relatively high, complicating the state of stress and introducing the possibility of bearing or crushing failure at the loading points. Thus, a very complex and difficult-to-define state of stress actually exists in the specimen, making the correlation of an applied load to an actual shear strength questionable" [30 p.340]. These findings, as well as the results from the photomicrographs for the fibercomposite specimens, conclude that the short beam test is not an accurate measure of the shear strength of fibercomposite materials because of the stress concentrations that are occurring throughout the beam specimen.

3.5.1.2. Torsion of a solid round bar

The torsion test of a solid round bar involves a round bar with a torque applied to one end while the other end is torsionally supported. Figure 3.3 illustrates the torsion of a solid round bar. A simple equation can be used to determine the shear stress occurring on the surface of the round bar as given in Equation 3.2.

$$\tau_{(maximum)} = \frac{2T}{\pi R^3}$$
Eqn. 3.2

where:

T = Torque applied (in-lb)
R = Radius of bar (in.)

This test can determine the stress occurring in the rod up to the proportional limit if the fibers are parallel to the axis of the specimen [30]. Unfortunately, for this research project, this test method does not accurately model the transverse loading situation occurring in the pavement dowel bar. Additionally, the use of this test would require a separate testing frame and the problems of developing a method to grip the dowel bars would have to be addressed. For these reasons, torsion of a solid rod shear
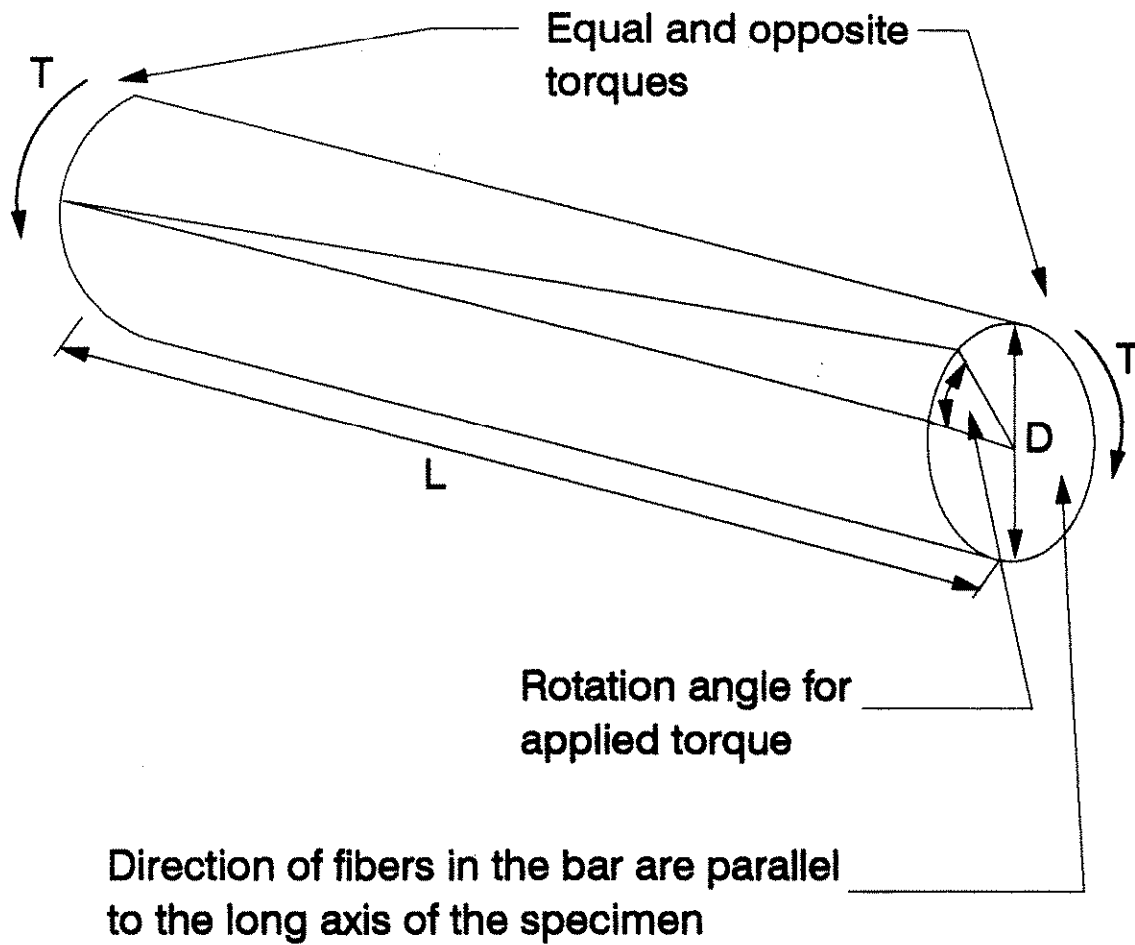
Figure 3.3. Illustration of the torsion of a solid round bar
shear test

test was not developed for this research program.

3.5.1.3. Iosipescu shear test method

The Iosipescu shear test achieves a state of pure shear loading at the centerline of the specimen by its geometry [31]. The load is applied in such a way that the shear is constant in the region at the centerline of the dowel and the moment is very small, in fact is zero, at the centerline of the specimen [31,32]. Figure 3.4 illustrates the force, shear and moment diagrams for the Iosipescu shear test method.

The controlling idea behind the test is that "each end of the test specimen is restrained from rotating by the loading fixture and simultaneously undergoes shear loading" [31:p.106] (see Figure 3.4). In addition to the development of this test procedure, Iosipescu also discovered "that by cutting 90-degree notches on each edge of the specimen, the shear stress distribution within the test specimen could be altered. By cutting these notches, the shear stress distribution can be changed from the parabolic shear stress distribution present in constant cross-section beams to constant shear stress distribution in the region between the two notches" [31:p.107]. The notched Iosipescu specimen is shown in Figure 3.5.

The Iosipescu shear test method was selected for the Iowa State research program for three main reasons:

1) The loading resulting from the test procedure is nearly identical to the loading situation that a pavement dowel would experience in the field.
2) If the shear stress reaches the limiting value, the specimen will fail in shear. Shear tests that do not result in the shear failure of the specimen are not an accurate measure of the material's shear strength.
3) The loading situation is such that large stress concentrations resulting from the application of the load over a relatively large area are avoided.

To utilize the Iosipescu shear test method, the test frame used for this research project was constructed based on the smaller Iosipescu test frames developed by Adams at the University of Wyoming [31]. The test fixture used by Adams was made for very small test specimens. This research project required a much larger frame. However, the geometry of the loading and support systems are the same. Figure 3.4 shows a schematic of the frame used by Adams at the University of Wyoming. Figure 3.6 shows a schematic of the frame developed in this research project for testing the relatively large dowel specimens.
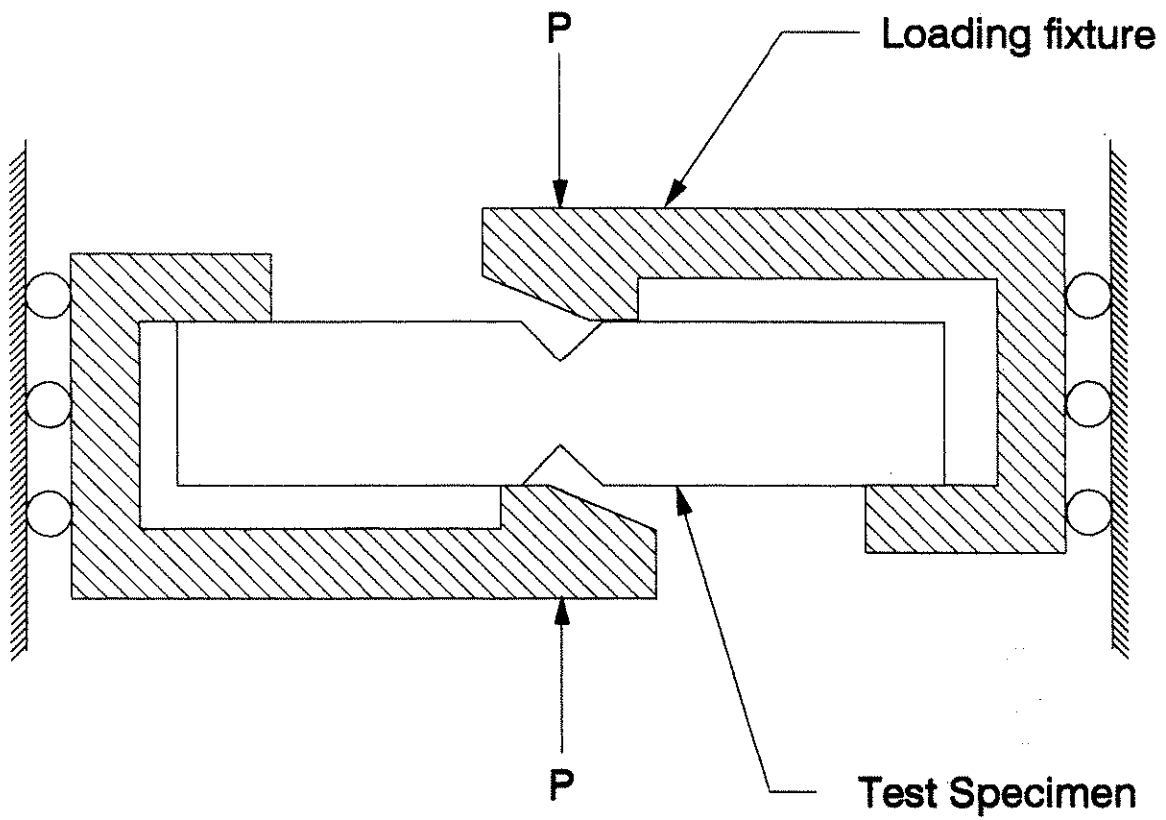
P

Loading fixture

P

Test Specimen

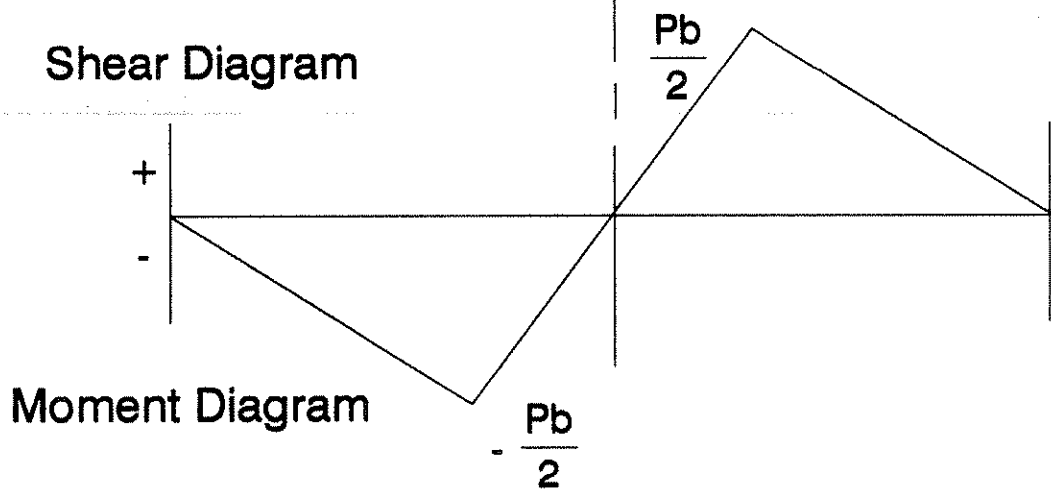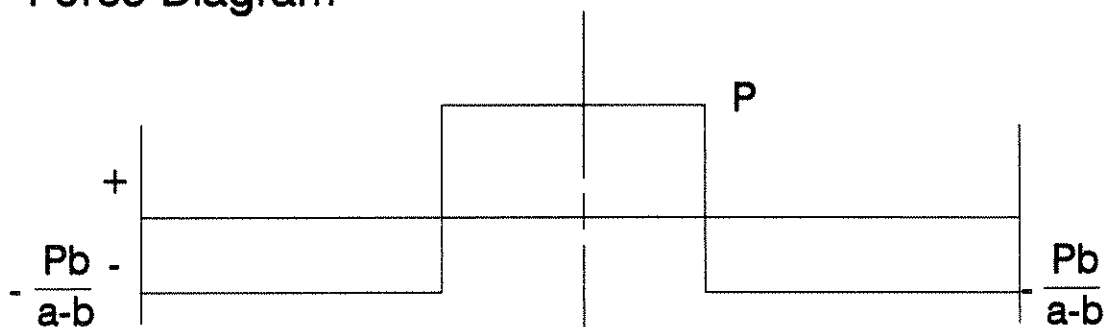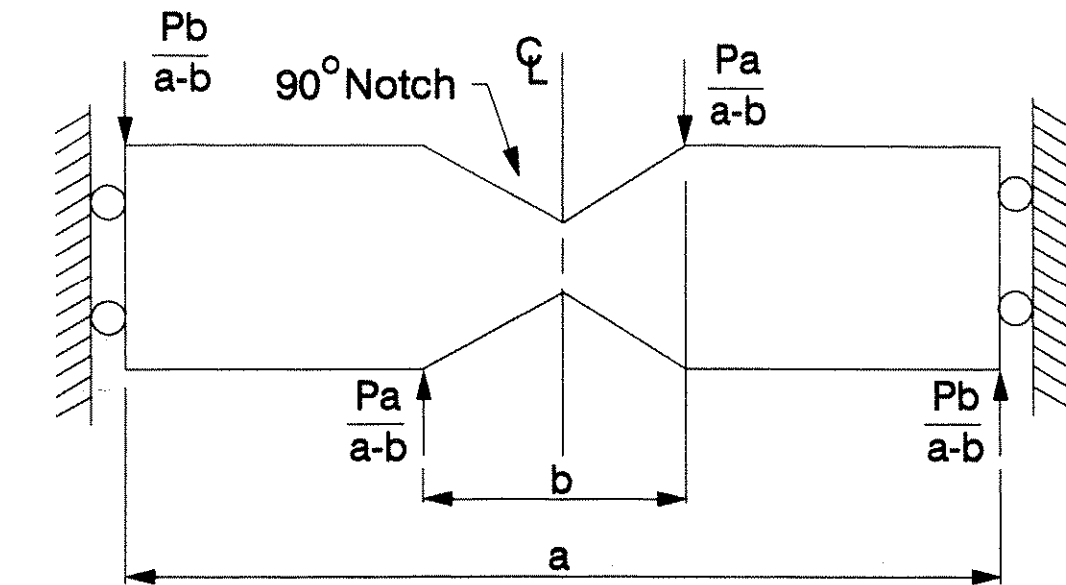Figure 3.4. Schematic of Adam's Iosipescu test
frame [31]

Figure 3.5. Force, shear, and moment diagrams for the Iosipescu shear test [31]
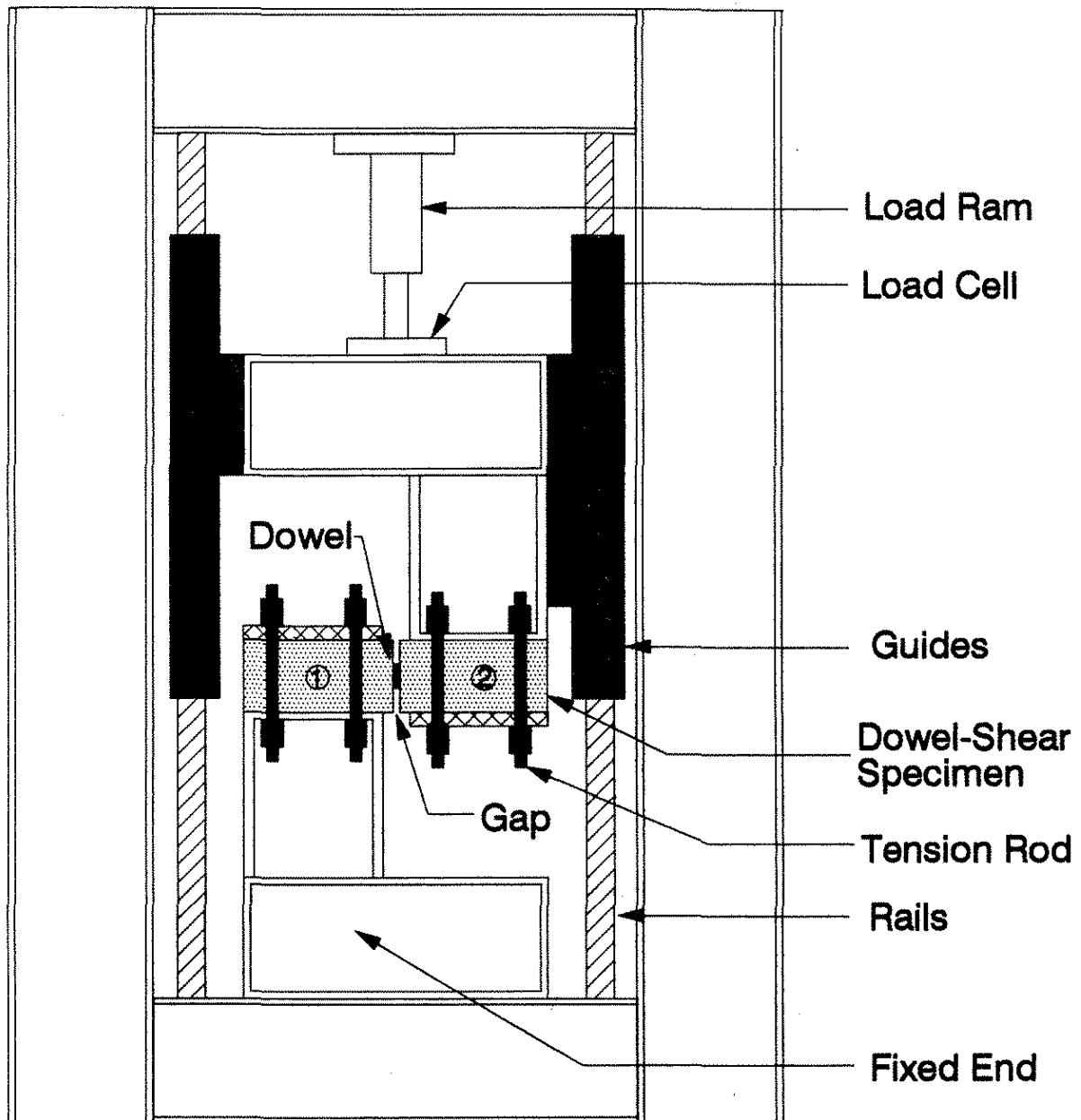
Figure 3.6. ISU dowel-shear frame

The dowel-shear specimen was held securely by tension rods (refer to Figure 3.6) to minimize bending and rotation of the assembly during testing. One half of the specimen (designated by Side 1 in Figure 3.6) was anchored to the fixed end of the frame while the force (applied by a hydraulic ram) was transferred through the other side (designated by Side 2 in Figure 3.6) resulting in direct shear of the dowel bar. The gap (refer to Figure 3.6), as explained early in this report, helped transfer the force through the dowel bar from one side of the specimen to the other without aggregate interlock or interface friction.

The graphs in Appendix A, for the dowel-shear specimens, reflect the differential deflection between Sides 1 and 2 (see Figures 3.6 and 3.7) versus load.
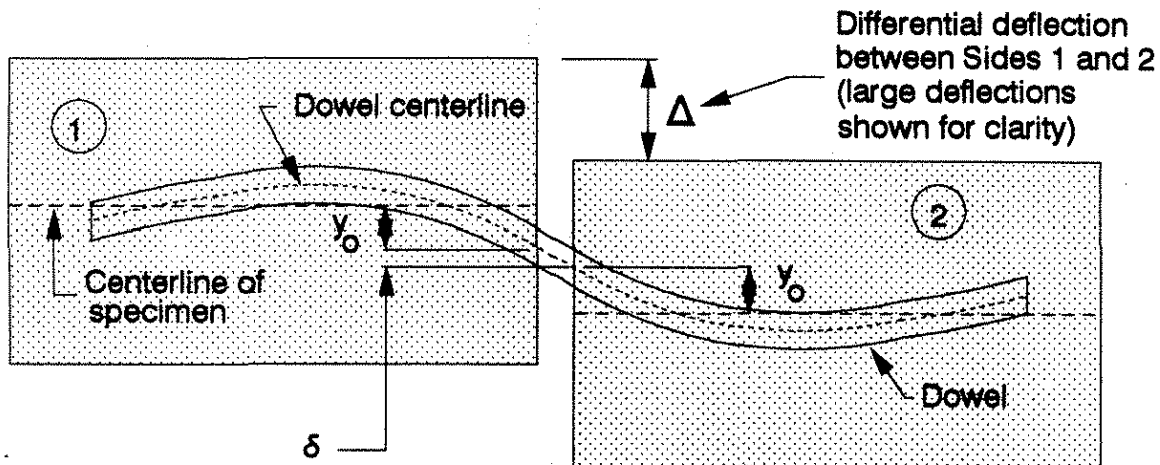
Figure 3.7. Differential deflection in dowel specimen

3.6. Results

The results of the testing program are presented in this section based upon the performance of individual or a series of specimens. A description of the specimen identification system used for each test series may be found in Figure 3.8. A representative curve of the Figures in Appendix A is given in Figure 3.9. and is discussed in the text below.

The graphs given in Appendix A are shown by a representative curve in Figure 3.9. This curve shows three regions (A,B and C) which are typical of all tests in this series. Region A (see Figure 3.9.) shows the elastic portion of the curve and is characterized by bending of the dowel. Bending of the dowel
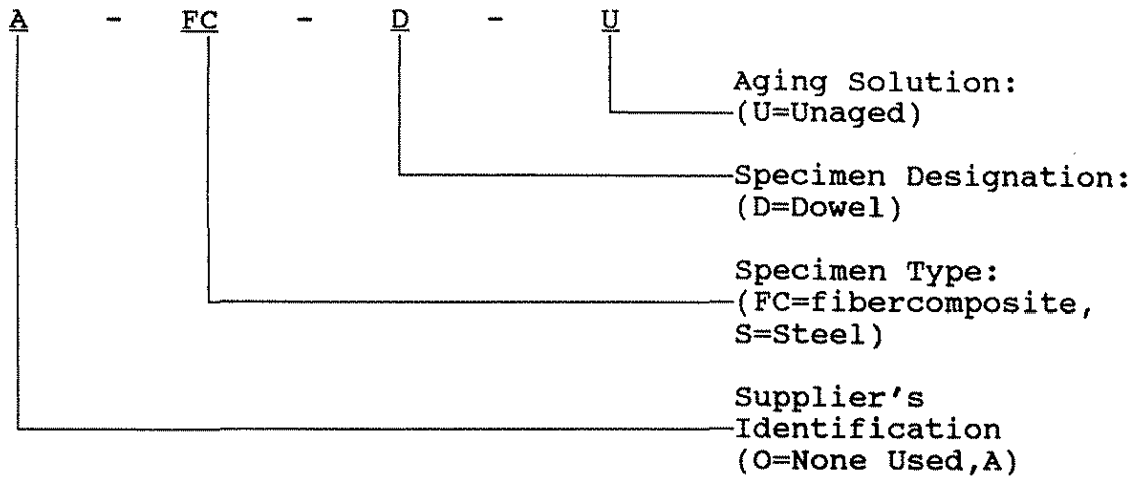
```
A    -    FC    -    D    -    U
|         |         |         |
|         |         |         |_____ Aging Solution:
|         |         |          _____(U=Unaged)
|         |         |
|         |         |_____Specimen Designation:
|         |                           (D=Dowel)
|         |
|         |_____Specimen Type:
|                                       (FC=fibercomposite,
|                                        S=Steel)
|
|_____Supplier's
                                          Identification
                                          (O=None Used,A)
```

Figure 3.8. Specimen identification system

continued to occur until cracking of the concrete. This concrete cracking marked the beginning of Region B (see Figure 3.9.) where the dowel specimen continued to carry load (and in some cases increasing load). The dowel specimen continued to carry load due to the clamping force applied by the testing frame (Refer to Figure 3.6). Final failure of the concrete resulted in substantial loss of load-carrying capacity as shown in Region C (see Figure 3.9).

The data resulting from the test matrix is represented in graphical form, and can be found in Appendix A, Figures A1 and A2. The graphs show a load versus deflection curve for five different specimens in each test series. Series 1 and 2 represent testing of FC dowel specimens and steel dowel specimens, respectively.

The Reasonably Expected Elastic Load (REEL) and associated deflections are given in Table 3.3 and correspond to REEL values taken from the graph in Appendix A. The REEL values indicate the end of the elastic region (initial straight line portion of the graph) and the start of the inelastic region. As discussed in Figure 3.9, the REEL load marked the beginning of the concrete cracking. This concrete failure was restrained by the clamping forces applied by the testing frame. The peak loads (PL) will be therefore taken as the REEL loads given in Table 3.3.

These combined PL and REEL loads can be used to obtain the shear stress in the dowel bars. The maximum shear stress for the Iosipescu shear test (for unnotched specimens) is determined through the use of the elementary beam theory equation:

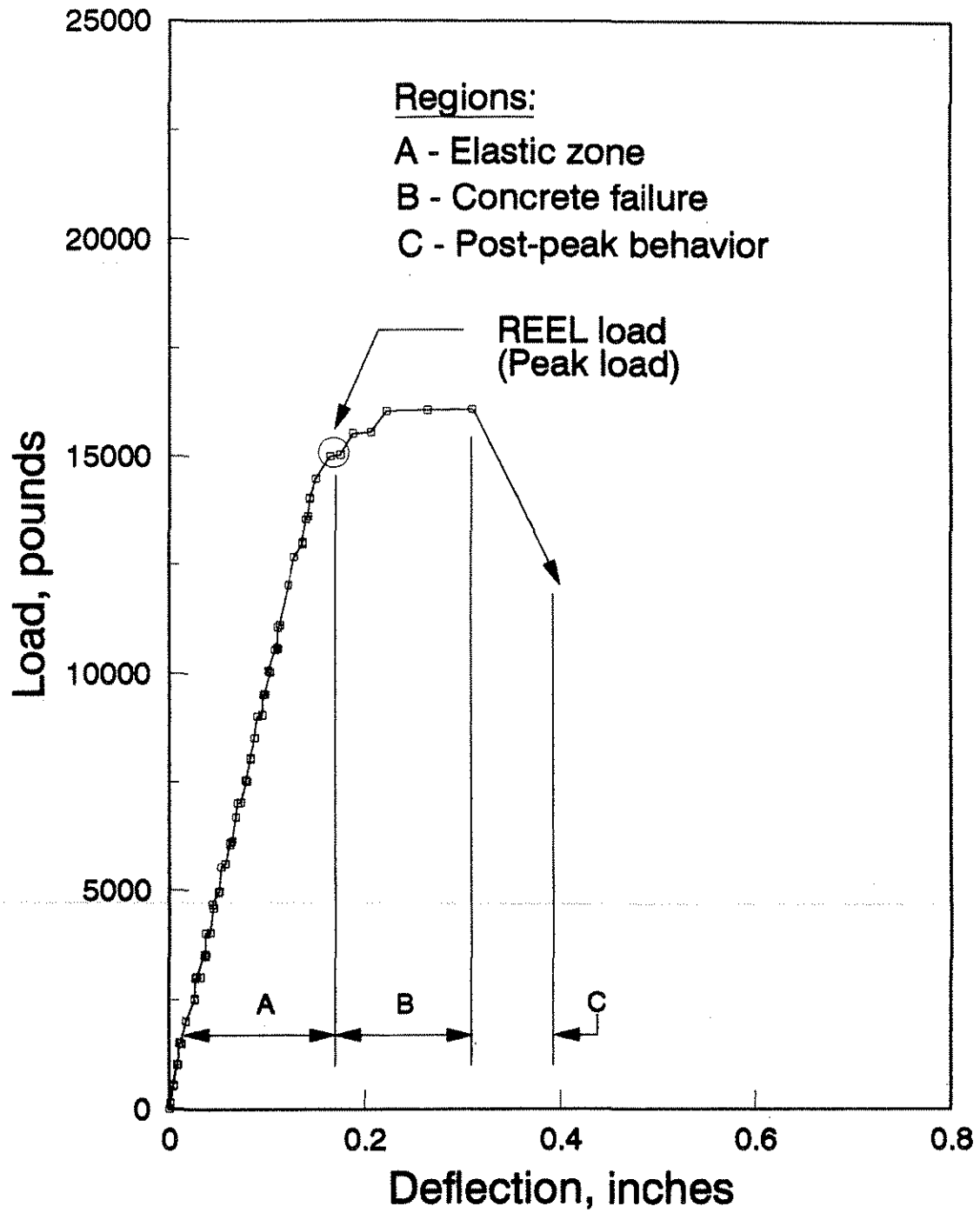$$\tau_{(maximum)} = \frac{V}{A_d}$$

Eqn. 3.3

Figure 3.9. Representative load–deflection curve

The average stiffness associated with the elastic portion of each load-deflection curve is given in Table 3.4. The stiffness was determined by calculating the slope of the line between 20 and 80 percent of REEL.

Table 3.3. Dowel REEL and deflection results

Assembly	Trial 1 REEL (lbs) (in.)	Trial 2 REEL (lbs) (in.)	Trial 3 REEL (lbs) (in.)	Trial 4 REEL (lbs) (in.)	Trial 5 REEL (lbs) (in.)	Avg. REEL (lbs) (in.)
A-FC-D-U (Fig A1)	17067 0.201	14894 0.186	12005 0.139	12664 0.128	12613 0.133	13849 0.157
O-S-D-U (Fig A2)	17810 0.012	18982 0.015	18059 0.016	18402 0.015	17998 0.017	18250 0.015

Table 3.4. Dowel specimen stiffness

Assembly	Trial 1 Stiff. *	Trial 2 Stiff. *	Trial 3 Stiff. *	Trial 4 Stiff. *	Trial 5 Stiff. *	Avg. Stiff. *
A-FC-D-U	88.3	79.0	87.0	99.4	95.3	89.8
O-S-D-U	1307	1410	1250	1281	1400	1330

* Units given in kips/in.

4.0. Analysis of Experimental Results

4.1. Dowel Deflection at the Face of the Joint

If Δ is the total relative deflection of the two slabs at a joint and δ is the shear deflection of that part of the dowel contained in the joint opening, the deflection of the dowel relative to concrete in one of the slabs is given by

$$y_o = \frac{(\Delta - \delta)}{2}$$
Eqn. 4.1

The total relative deflection, Δ is measured experimentally whereas the shear deflection, δ is obtained from the following expression, [33]

$$\delta = \frac{F P_t L_s}{A_d G}$$
Eqn. 4.2

where:
F = form factor, equal to 10/9 for solid circular section
P_t = dowel shear (lbs)
L_s = shear span of the dowel within the joint opening (in.)
A_d = area of dowel (in²)

$$G = \frac{E}{2(1+\mu)}$$ = shear modulus (psi)

This expression for shear modulus, G, is not valid for fibercomposite materials because of the anisotropic material behavior. But since the shear deflection is very small when compared to the relative deflection, large variation in the value G does not have considerable effect on the results of analysis. Hence, the above classical expression for G was used in the current work. More scientific procedure for establishing the value of shear modulus for FC material is presently being studied.

Table 4.1 lists the total relative deflection, shear deflection and deflection of the dowel relative to the concrete under a dowel shear of 10,000 lb for various 1.5-inch steel dowel specimens. Table 4.2 gives the corresponding values for 1.25-inch FC dowel specimens. A modulus of elasticity of 6,000 ksi and poisson's ratio of 0.25 was used in this regard. The value of the dowel shear used to calculate the values of y_o is arbitrary, but the same value of P_t should be used while graphing the relationship

between k_o and y_o.

Table 4.1. Experimental deflection of 1.5 in. dia. steel dowel
specimens under 10,000 lb shear

Specimen No.	Total relative deflection, Δ(in.)	Shear deflection, δ (in.)	Dowel deflection at the face of the joint, y_o (in.)
S1	0.00765	0.0000704	0.00379
S2	0.00709	0.0000704	0.00351
S3	0.00800	0.0000704	0.00396
S4	0.00781	0.0000704	0.00387
S5	0.00714	0.0000704	0.00353
Average value of y_o =			0.00373

Table 4.2. Experimental deflection of 1.25 in. dia. FC dowel
specimens under 10,000 lb shear

Specimen No.	Total relative deflection, Δ(in.)	Shear deflection, δ(in.)	Dowel deflection at the face of the joint, y_o(in.)
F1	0.116	0.0004714	0.0578
F2	0.123	0.0004714	0.0613
F3	0.114	0.0004714	0.0568
F4	0.106	0.0004714	0.0528
F5	0.105	0.0004714	0.0523
Average value of y_o =			0.0562

4.2. Modulus of Dowel Support

Separate k_o versus y_o graphs were developed for steel and FC
dowel systems at a dowel shear of 10,000 lb. The development of
these graphs was based on the finite beam idealization of the
dowel-concrete system. The process of developing these graphs
involved establishing the deflection equation for a particular

value of k_o, substituting x=0 in the equation for deflection to get the value of y_o, and repeating the same for various values of k_o. Graphs relating k_o and y_o are presented in Figures 4.1a and 4.1b for 1.5-inch diameter steel and 1.25-inch diameter FC dowels, respectively.

The specific values of modulus of dowel support corresponding to the experimental values of y_o were obtained from these graphs. The values were checked numerically, and tabulated in Table 4.3 for 1.5-inch diameter steel and 1.25-inch diameter FC dowels.

4.3. Deflection Equation

The establishment of deflection equations for the two-dowel systems was based on the solution of the finite beam problem presented in Section 2.3.2. The solution was worked out for an assumed dowel shear, P_t of 10,000 lb. The moment in the dowel at the face of the joint, M_o was calculated as :

$$M_o = -\frac{P_t Z}{2} = -\frac{10000\left(\frac{1}{8}\right)}{2} = -625\, lb\text{-}in. \qquad \text{Eqn. 4.3}$$

Experimental k_o values were read from Table 4.3, and the length of the finite beam, L was taken as 9" (length of the dowel on one side of the joint).

Table 4.4 presents the solution of the finite beam problem in terms of the constants A, B, C and D defining the deflection equations for steel and FC dowel systems. Using these constants, the equation for deflection along the dowel was established for steel and FC dowels. Figures 4.2a and 4.3a show the corresponding deflection diagrams.

4.4. Bending Moment, Shear Force and Pressure

The distribution of bending moment and shear force along the length of the dowel were obtained from the second and third differentials of the deflection equation given by Equations 2.18 and 2.19. Differentiation of Equation 2.19 yields the fourth differential of the deflection equation from which the equation for pressure along the length of the dowel was obtained.

With the values of A, B, C and D taken from Table 4.4, the distributions of bending moment, shear force and pressure along the dowel were obtained, and the same were graphed and presented in Figures 4.2 and 4.3.
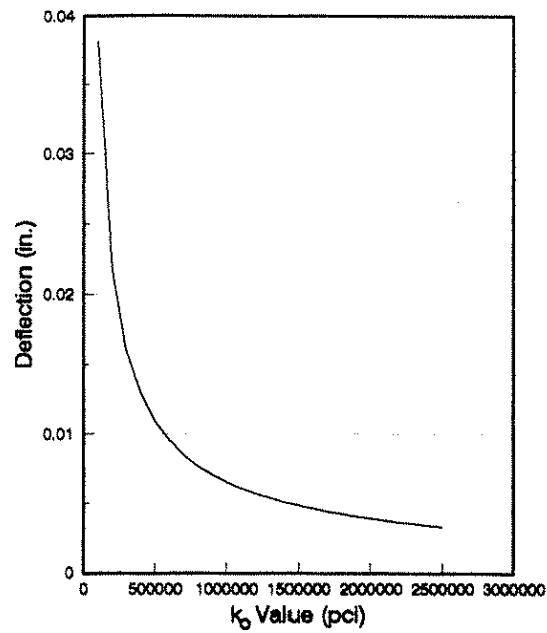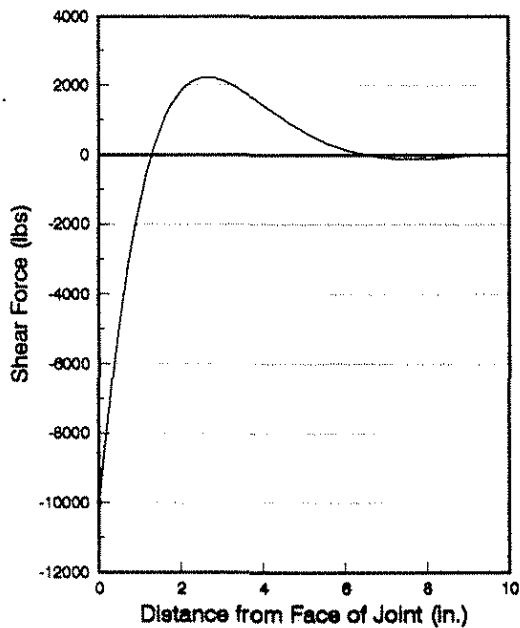
a. 1.5 in. dia. steel dowel
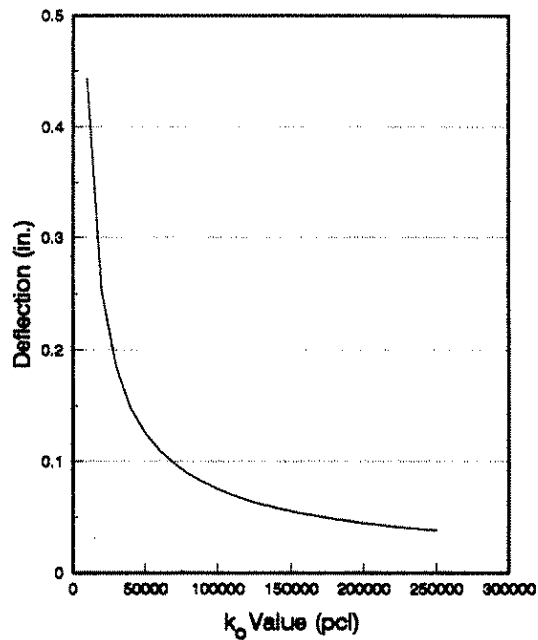
b. 1.25 in. dia. FC dowel

Figure 4.1. Modulus of dowel support, k_o versus deflection of dowel at the face of the joint, y_o
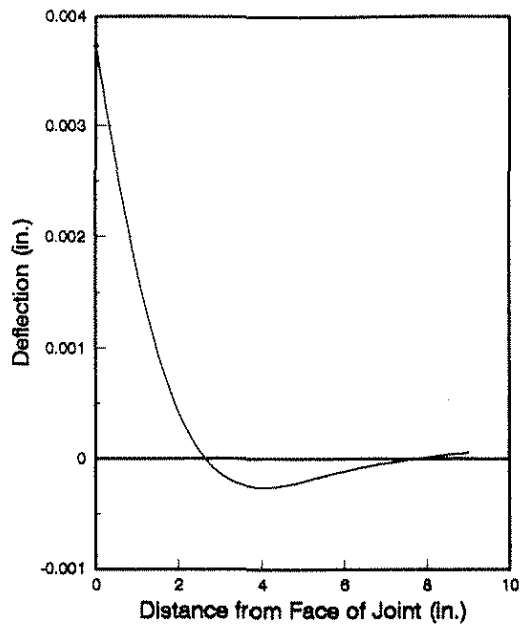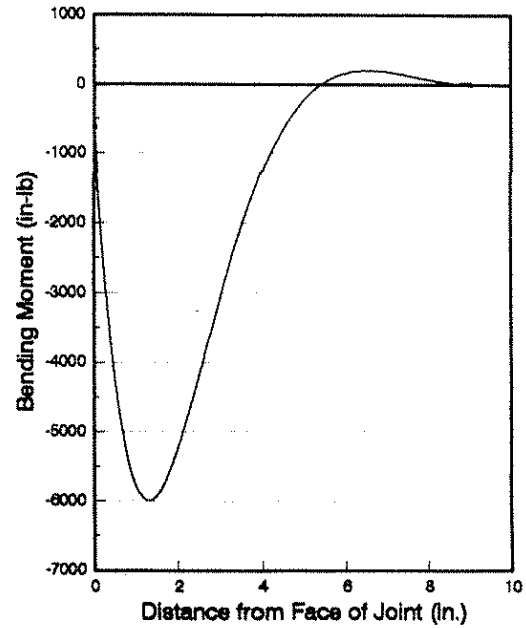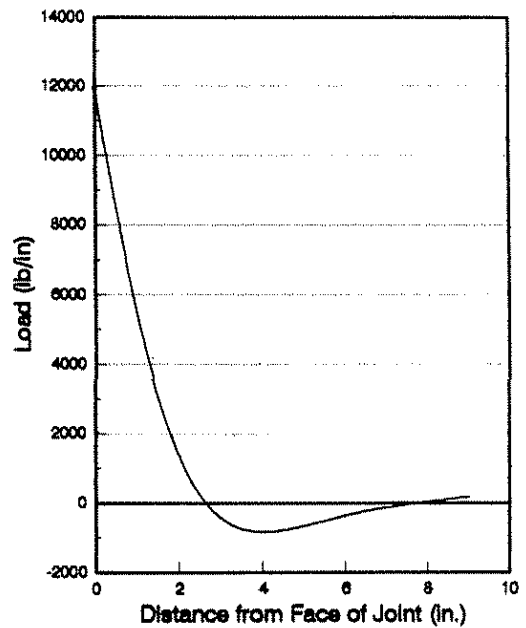
a. Deflection

b. Bending Moment

c. Shear Force

d. Load

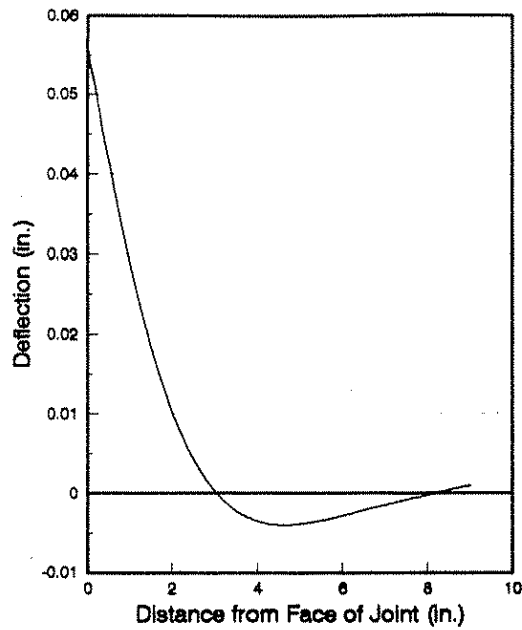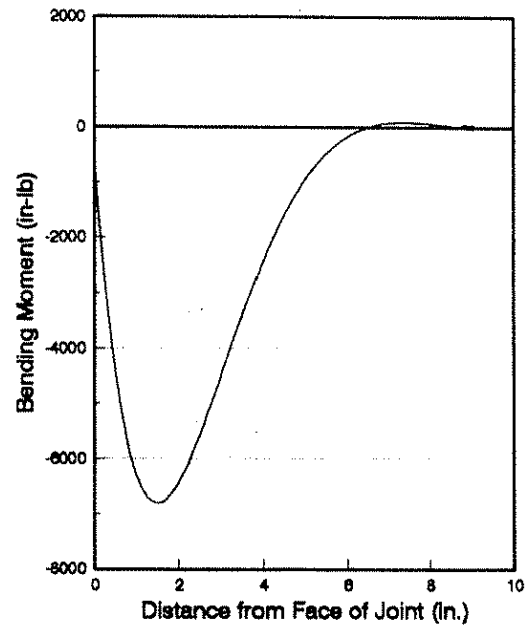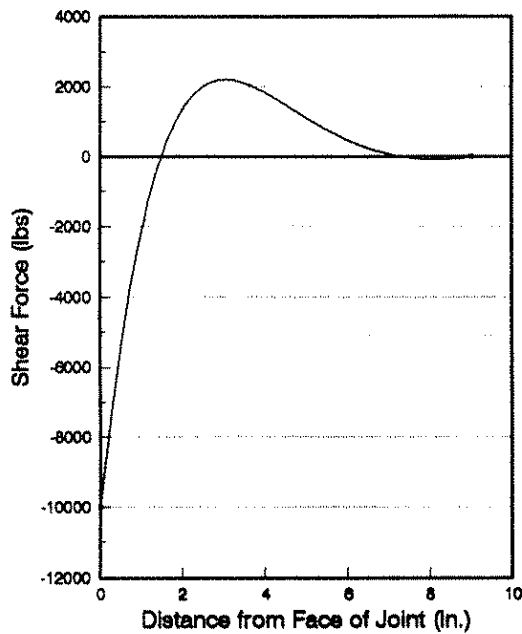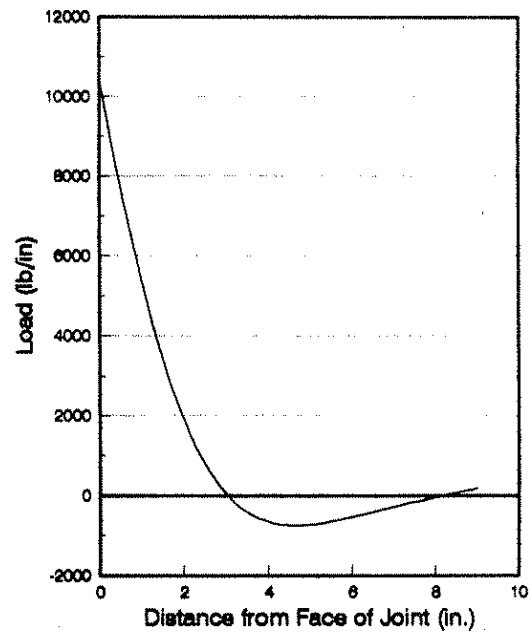Figure 4.2. Results of analysis of 1.5 in. dia. steel dowel

42

a. Deflection

b. Bending Moment

c. Shear Force

d. Load Diagram

Figure 4.3. Results of analysis of 1.25 in. dia. FC dowel

Table 4.3. Experimental values of k_o

Specimen	Average value, y_o (in.)	Value of k_o (pci)
1.5" steel dowel	0.00373	2139000
1.25" FC dowel	0.0562	148180

Table 4.4. Results of finite beam analysis problem

Specimen	A	B	C	D
1.5" steel dowel	2.064E-07	-1.79E-07	3.731E-03	-1.30E-04
1.25" FC dowel	4.196E-06	-1.28E-05	5.613E-02	-1.72E-03

4.5. Critical Stresses

4.5.1. 1.5" steel dowel specimen

Bearing stress in concrete,

$$\sigma = k_o y_o = 2139000 * 0.00373 = 7978 psi \qquad \text{Eqn. 4.4}$$

Shearing stress in dowel,

$$\tau = \frac{P_t}{\frac{\pi d^2}{4}} = \frac{10000}{\frac{\pi (1.5)^2}{4}} = 5656 psi \qquad \text{Eqn. 4.5}$$

Bending stress in dowel,

$$f = \frac{M_{max}}{S} = \frac{6000}{\frac{\pi (1.5)^3}{32}} = =18101 psi \qquad \text{Eqn. 4.6}$$

4.5.2. 1.25" FC dowel specimen

Bearing stress in concrete,

$$\sigma = k_o y_o = 148180 * 0.0562 = 8328 psi \qquad \text{Eqn. 4.7}$$

Shearing stress in dowel,

$$\tau = \frac{P_t}{\frac{\pi d^2}{4}} = \frac{10000}{\frac{\pi (1.25)^2}{4}} = 8145 psi \qquad \text{Eqn. 4.8}$$

Bending stress in dowel,

$$f = \frac{M_{max}}{S} = \frac{7000}{\frac{\pi (1.25)^3}{4}} = 36492 psi \qquad \text{Eqn. 4.9}$$

Table 4.5. Critical stresses

Specimen	σ (psi)	τ (psi)	f (psi)
1.5" steel dowel	7978	5656	18101
1.25" FC dowel	8328	8145	36492

5.0. Conclusions

As stated previously, this is Part 1 of a two-part final report.   Part 1 covers development of the experimentation procedures and the theory for analyzing effects of accelerated aging on the shear behavior and strength of fibercomposite (FC) dowels and on the bond behavior of FC reinforcing bars. A direct strength comparison of the steel dowels to the FC bars is contained in both Parts 1 and 2.

Different theoretical models for the analysis of dowels were investigated and developed. Timoshenko's analysis was concluded to be the most appropriate method.   A solution to the finite beam problem, as opposed to the conventional semi-infinite solution was considered and presented in Section 2.3.   Figures 5.1 and 5.2 demonstrate a comparison between the results obtained from the analysis using the developed theoretical model and those results of analysis using the semi-infinite idealization.

The experimental investigation yielded results establishing maximum strengths, behavioral characteristics and failure modes. The maximum strengths were based upon a reasonably expected elastic load (REEL).   The average value of REEL observed for the FC dowel specimens was 13,849 lb. compared with a typical required maximum service load of 4500 lb.   The maximum bending moment in the FC dowel was observed to be 7000 lb-in resulting in a fiber stress value of 56,506 psi which is less than the ultimate coupon flexural stress of 100,000 psi [13].
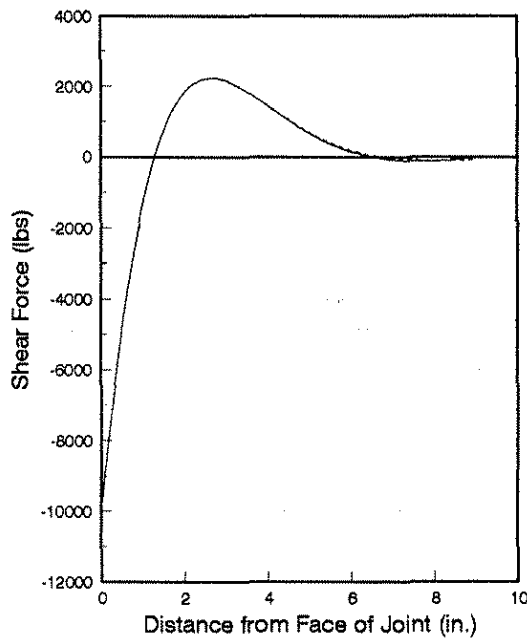
Further testing is recommended for establishing the values of modulus of dowel support for various ranges of concrete compressive strength and dowel diameters.   These results could be used to generalize the analysis for accommodation of all types of dowel systems, including possible non-circular dowel sizes.
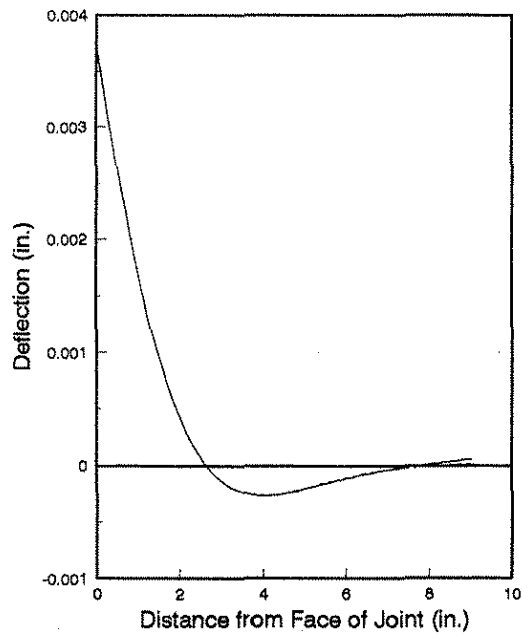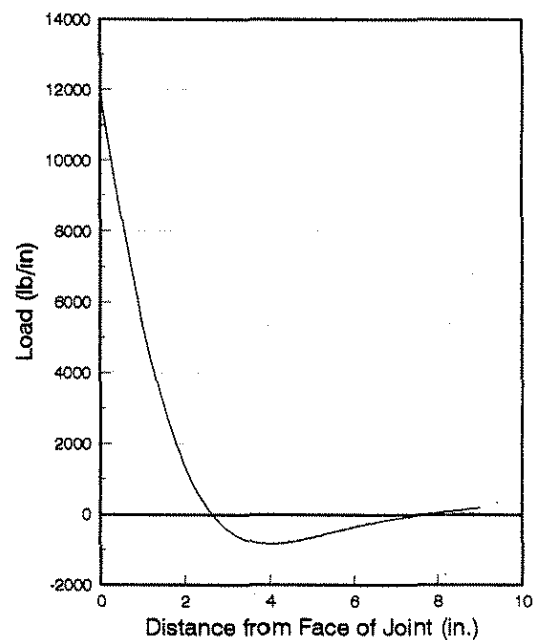
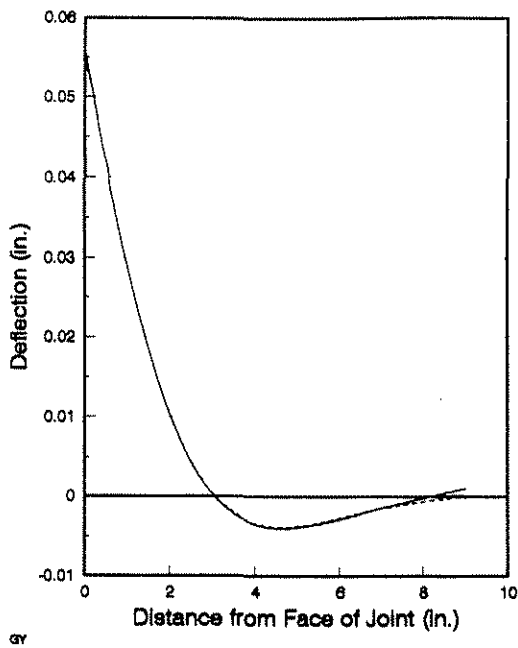a. Deflection
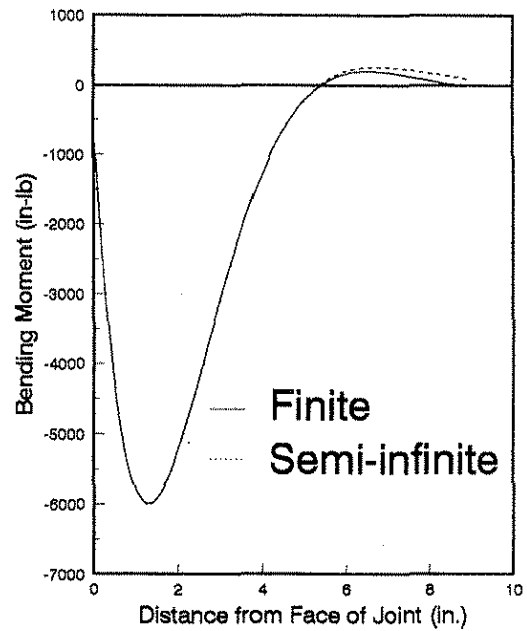
b. Bending Moment
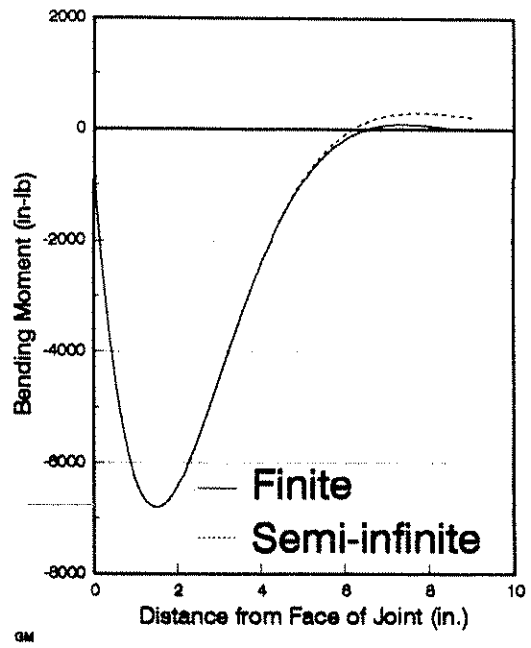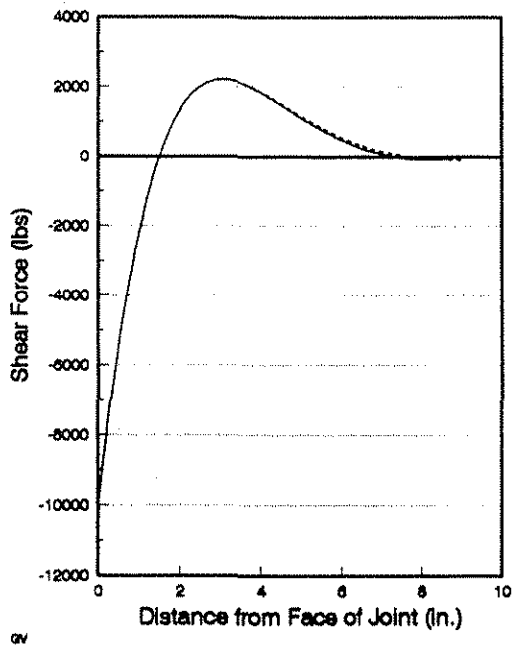
c. Shear Force

d. Load

Figure 5.1. Results of analysis of 1.5 in. dia. steel dowels
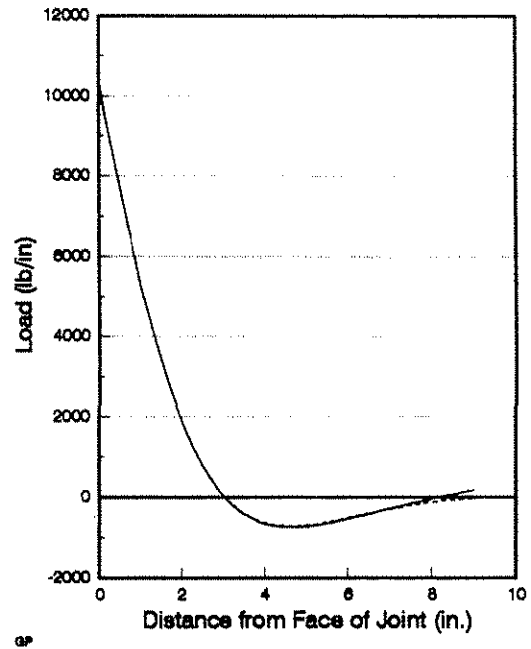   -comparison between Finite & Semi-infinite solutions

(a) Deflection

(b) Bending Moment

(c) Shear Force

(d) Load

Figure 5.2. Results of analysis of 1.25 in. dia. FC dowels
            -comparison between Finite & Semi-infinite solutions

48

6.0. Acknowledgements

References

1. Porter, M.L., Proposal to Iowa Department of Transportation, "Thermoset Composite Concrete Reinforcement", Iowa State University, Engineering Research Institute, Ames, Iowa, November 1989.

2. Snyder, Mark B., Reiter, Micheal J., Hall, Kathleen T., and Darter, Michael I., Rehabilitation of Concrete Pavements, Volume I: Repair Rehabilitation Techniques FHWA-RD-88-071. McLean, VA: Research, Development, and Technology Turner-Fairbank Highway Research Center, 1989.

3. Babaei, Khossrow, and Hawkins, Neil M., Evaluation of Bridge Deck Protective Strategies-NCHRP Report 297. Washington, D.C.: Transportation Research Board, September 1987.

4. Clear, Kenneth C., "Effectiveness of Epoxy-Coated Reinforcing Steel", Concrete International, May 1992, pages 58-64.

5. Corbo, Vincent, "Advanced Materials Geared for the 90s", Design News, January 1990, pages 69-70.

6. Brown, Gordan, "Fiber Glass Scores with Designers", Design News, November 1988, pages 258-262.

7. Plecnik, J.M., and Ahmad, S.H., "Transfer of Composite Technology to Design and Construction of Bridges", Interim Report prepared for U.S. Department of Transportation. Washington, D.C.: North Carolina State University, 1985.

8. Bakeri, P.A., "Analysis and Design of Polymer Composite Bridge Decks", Master's Thesis. Massachusetts Institute of Technology, Cambridge, MA, 1989.

9. Long, Bob. Personal Interviews. Ames, Iowa: Composite Technologies Corporation, 1990-1991.

10. Whitney, James M., Daniel, Issac M., and Pipes, Byron R., Experimental Mechanics of Fiber Reinforced Composite Materials. Brookfield Center, CT: Society for Experimental Stress Analysis Monograph Series, 1982.

11. Composite Technologies Corporation. Advertising Brochure on Fibresteel. Ames, Iowa: Composite Technologies Corporation, 1990.

12. Medical Center Hospital, San Antonio, Texas, Reynolds-Schlattner-Chetter-Roll, Inc. 1985.

13. Morrison Molded Fiberglass Company, Extern Design Manual, Bristol, Virginia, 1989.

14. Richard, D., Roll, "Use of GFRP Rebar in Concrete Structures", <u>Advanced Composite Materials in Civil Engineering Structures</u>, Proceedings of the Speciality Conference, American Society of Civil Engineers, Las Vegas, Nevada, 1991, pages 93-98.

15. Wade, G.T., Porter, M.L., and Jacobs, D.R., <u>Glass Fiber Composite Connectors for Insulated Concrete Sandwich Walls</u>. Ames, IA: Iowa State University Engineering Research Institute, March 1988.

16. Westergaard, H.M., "Spacing of Dowels", proceedings, 8th Annual Meeting of the Highway Research Board, Washington, D.C., 1928, pages 154-158.

17. Yoder, E.J., and Witczak, M.W., "Principles of Pavement Design", second edition, John Wiley & Sons, Inc., 1975.

18. Friberg, B.F., "Design of Dowels in Transverse Joints of Concrete Pavements", proceedings, American Society of Civil Engineers, Vol. 64, part-2, 1938, pages 1809-1828.

19. Westergaard, H.M., "Computation of Stresses in Concrete Roads", proceedings, part I, Highway Research Board, 1925, pages 90-112.

20. Tabatabie, A.M., "Structural Analysis of Concrete Pavement Joint", Ph.D. Thesis, University of Illinois, 1978.

21. Tabatabie, A.M., Barenberg, E.J., and Smith, R.E., "Longitudinal Joint Systems in Slip-Formed Rigid Pavements", Report No. FAA-RD-79-4, II, 1979.

22. Anstasios, M.I., Michael, I.D., Ming-Jen, L., and Kurt, W.H., "Joint Design Guidelines for Load Transfer and Spacing", Draft Report Prepared for US Department of Transportation, Federal Highway Administration, Prepared by Department of Civil Engineering, University of Illinois, 1987.

23. Bradbury, R.D., "Design of Joints in Concrete Pavements", proceedings, Highway Research Board, 1932, pages 105-136.

24. Timoshenko, S., "Strength of Materials - part II", 3rd edition, Robert E. Krieger Publishing Company, Huntington, New York, 1976.

25. Timoshenko, S., and Lessels, J.M., "Applied Elasticity", Westinghouse Technical Night School Press, Pittsburgh, Pennsylvania, 1925.

26. Porter, M.L., Albertson, M.D., Barnes, B.A., "Thermoset Concrete Reinforcement: Progress Report for   1990", Iowa State University, Engineering Research Institute, Ames, IA., 1990.

27. Whitney, J.M., and Browning, C.E., "On Short-Beam Shear Tests for Composite Materials." Experimental Mechanics, September 1985: pages 294-300.

28. Johnson, Steve. Personal Interview in Ames, Iowa, with Boeing Structural Engineer for the 777 Wing Trailing Edge Division. March 19, 1991.

29. American Society for Testing and Materials. Annual Book of ASTM Standards. Philadelphia, PA: ASTM, 1984.

30. Adams, Donald F., and Thomas, Rodney L., "The Solid-Rod Torsion Test for the Determination of Unidirectional Composite Shear Properties." Textile Research Journal, April 1969, pages 339-345.

31. Walrath, D.E., and Adams, D.F., "The Iosipescu Shear Test as Applied to Composite Materials", Experimental Mechanics, March 1983, pages 105-110.

32. Adams, Donald F., and Walrath, David E., "In-Plane and Interlaminar Iosipescu Shear Properties of Various Graphite Fabric/Epoxy Laminates." Journal of Composites Technology & Research 9.3 (1987), pages 88-94.

33. Young, W.C., "Roark's Formulas for Stress and Strain", Sixth Edition, McGraw-Hill Book Company, 1989, page 202.
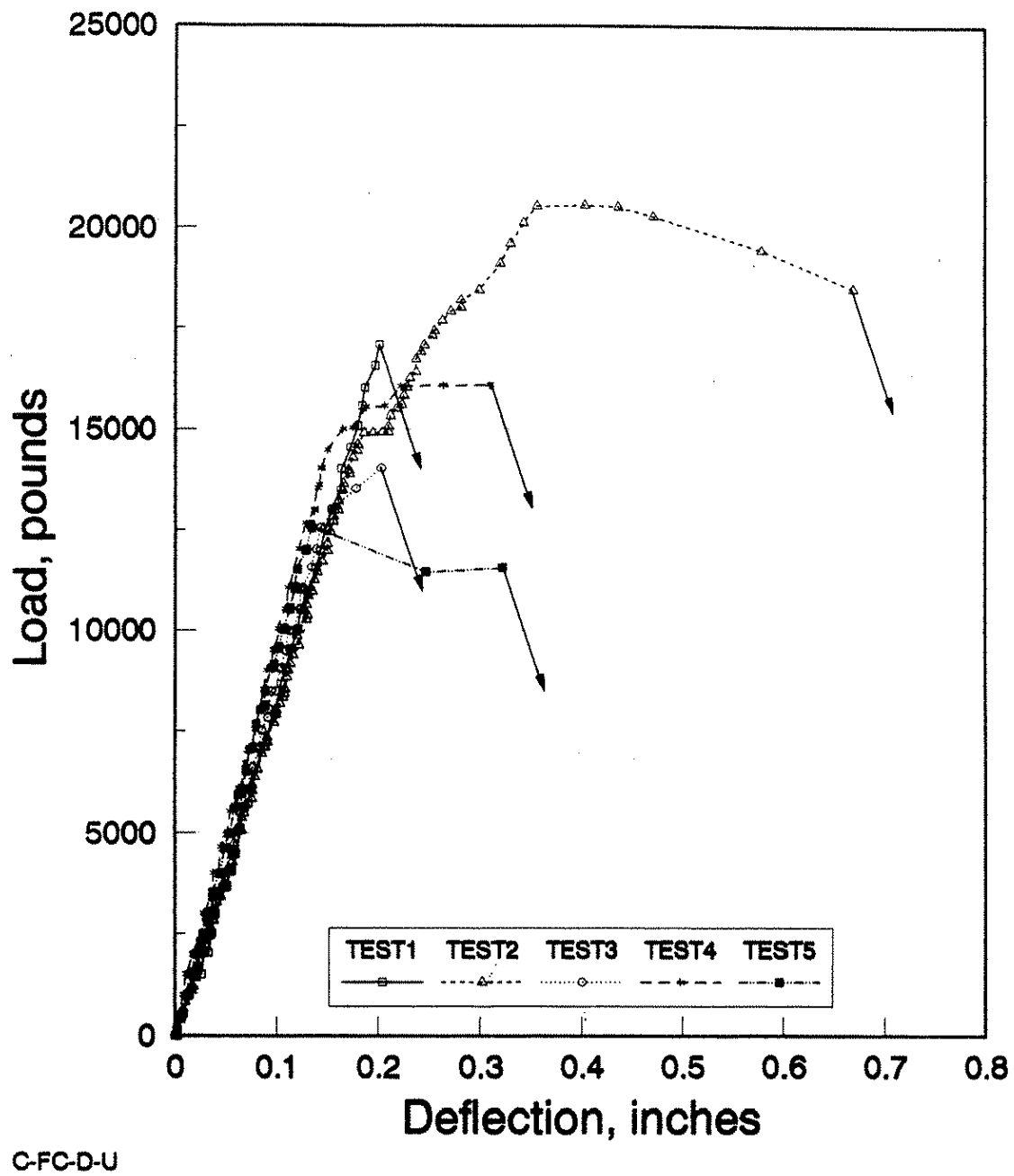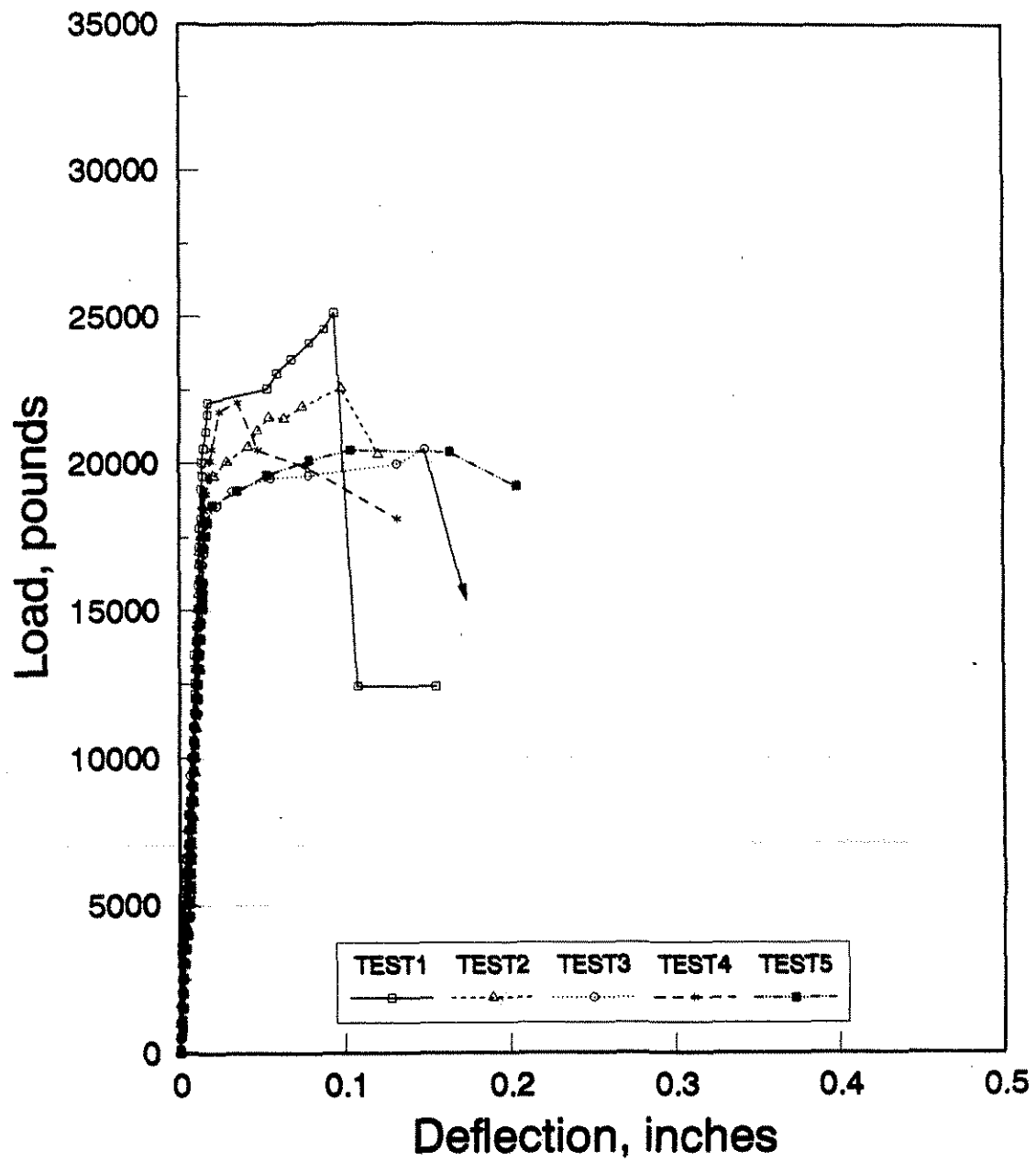
Appendix

DOT

C-FC-D-U

Figure A1. Unaged FC-dowel specimens (Supplier A)

DOT

O-S-D-U

Figure A2. Unaged steel-dowel specimens (Supplier O)